THE SOLVENT EFFECT ON THE ELECTRONIC STRUCTURE AND CHARGE TRANSPORT PROPERTIES OF CONJUGATED POLYMERS

HUDA HUSSIN

The Solvent Effect on the Electronic Structure and Charge Transport Properties of Conjugated Polymers

by

© Huda Hussin
B. Sc. (2006) 7th of April University

A thesis submitted to the
School of Graduate Studies
in partial fulfillment of the
requirements for the degree of
Master of Science.

Department of Physics and Physical Oceanography
Memorial University of Newfoundland

August 2011

St. John's Newfoundland

Contents

Abstract

The solvent effect on optical and electronic properties of conjugated polymers has recently been paid much attention. Conjugated polymers have many potential industrial applications, for example, they are used in optoelectronic devices such as organic light emitting diodes, field effect transistors, solar cells, and many others. In some cases it was shown that the usage of an appropriate solvent can lead to higher efficiency in organic solar cells. In this work, we investigate the solvent effect on the electronic structure properties of some conjugated polymers, basically, fluorene and carbazole oligomers, and some benzodithiophene based co-monomers. Also solvent effect on some transport properties of benzodithiophene based co-monomers are investigated. The energy levels, band gaps, and dipole moments are obtained with density functional theory (DFT). The B3LYP, hybrid exchange-correlation functional, and the polarized split-valance basis set, 6-31G^*, are used to determine optimized ground state structures of the above mentioned molecular systems. The time-dependant DFT is employed to calculate their excited state properties. For solvent effect we make use of the polarizable continuum model. Two solvents, chloroform and methanol are employed for fluorene and carbazole oligomers. Four solvents, chlorobenzene and o-dichlorobenzene, in addition to chloroform and methanol, are used for benzodithiophene based compounds. The results show that the presence of a solvent lowers the HOMO and LUMO energy levels, and increases or decreases the HOMO-LUMO

energy gap depending on the chemical system, and decreases the lowest excitation energy. The magnitude of ground state electronic dipole moment of the systems is increased in solutions. The solvent effect on the reorganization energy depends on the system studied. The calculated values for the various quantities are compared with the experimental ones whenever possible.

Acknowledgements

I would first like to thank my supervisor, Prof. J. Lagowski, for her appreciated help and her support over the two years of my graduate studies. I will never forget her way in supervising students, which will affect me for the rest of my education path. I would like to say thank you very much to her. In the Department of Physics and Physical Oceanography, I would especially thank Dr. Plumer, Dr. Whitehead, Dr. Lewis, and Dr. Yethiraj for their excellent lectures. I also like to thank the girls in the general office, Dr. Andrews, and Dr. de Young for their help and friendly personalities.

I really appreciate these people for helping me with computers. They are Fred Perry for his magic skills and immediate help whenever I needed it, Michelle Shaw for her help which I would not go so far without it. I also appreciate financial support from Canadian Bureau for International Education (CBIE) and the Natural Science and Engineering Council of Canada (NSERC). I would like to thank the Atlantic Computational Excellence Network (ACEnet), and Memorial University of Newfoundland for the use of their computational resources.

Finally, I would like a million thanks to my beloved husband for everything. I would not go any step forward in my study without his support and encouragement. I like to say: Thank you very much my great husband. Absolutely, I would send a huge thanks to my parents for making me very happy in my life.

Abbreviations

- **BHJ** Bulk Heterojunction
- **C** Carbazole
- **DFT** Density Functional Theory
- **DIO** 1,8-diiodooctane
- $\mathbf{E_1}$ Lowest Excitation Energy
- $\mathbf{E_{xc}}$ Exchange-Correlation Energy
- **EL** Electroluminescence
- **ETL** Electron Transport Layer
- **F** Fluorene
- **GGA** Generalized Gradient Approximation
- **HF** Hartree-Fock
- **HOMO** Highest Occupied Molecular Orbital
- **HTL** Hole Transport Layer
- **IPCM** Isodensity Polarized Continuum Model

- **ITO** Indium/Tin Oxide
- **LCAO** Linear Combination of Atomic Orbital
- **LDA** Local Density Approximation
- **LEDs** Light Emitting Diodes
- **LSDA** Local Spin Density Approximation
- **LUMO** Lowest Unoccupied Molecular Orbital
- **MM** Molecular Mechanics
- **OLED** Organic Light Emitting Diode
- **P3HT** Poly(3-hexylthiophene)
- **PA** Polyacetylene
- **PBnDT-DTBT** Poly[4,8-dialkylbenzo[1,2-b:4,5-b']dithiophene-4,7-di(2-thienyl)-2,1,3-benzothiadiazole]
- **PC** Polycarbazole
- **PCE** Power Conversion Efficiency
- **PCM** Polarizable Continuum Model
- **PES** Potential Energy Surface
- **PF** Polyfluorene
- **PLED** Polymeric Light Emitting Diode

- **PTB7** Poly[[4,8-bis[(2-ethylhexyl) oxy]benzo[1,2-b:4,5-b']dithiophene-2,6-diyl][3-fluoro-2-[(2-ethylhexyl) carbonyl]thieno[3,4-b] thiophenediyl]]
- **PTBs** Benzodithiophene Polymers
- **PVs** Photovoltiacs
- **QM** Quantum Mechanics
- **SCI-PCM** Self-Consistent Isodensity Polarized Continuum Model
- **SCRF** Self Consistent Reaction Field
- **TD-DFT** Time-Dependant Density Functional Theory
- **ZINDO** Zerner's Intermediate Neglect of Differential Overlap

List of Tables

List of Figures

Chapter 1

Introduction

1.1 Organic Conjugated Polymers

Organic conjugated polymers combine novel semiconducting electronic properties with the processing flexibility of polymers. π-electrons are delocalized along the polymer chain giving these materials a pseudo one-dimensional character [1]. The optical and electronic properties of organic conjugated polymers have led to their use in different applications including batteries, electrochromic devices, photovoltaics, and light-emitting diodes (LEDs) [2]. Conjugated polymers have flexibility, wide spectral range, and are easily patterned which make them competitive with their inorganic counterparts [1].

Electronic properties (such as the electrical conductivity) of conjugated polymers were discovered in 1977 [3] by Heeger, MacDiarmid, and Shirakawa when they showed that the conductivity of polyacetylene (PA) can be increased by several orders of magnitude by oxidation with iodine. For their discovery they were awarded the Nobel Prize in Chemistry in 2000 [4]. In early 1990's it was also discovered that conjugated polymers have optical properties such as electroluminescence and photoluminescence.

Many applications have been devised that make use of these electronic and optical properties of conjugated polymers. In the next two sections, we discuss in some detail two main applications of conjugated polymers, light emitting diodes due to their electroluminescence property, and photovoltaics due to their light conversion property. We briefly summarize the importance of solvents for these devices.

1.1.1 Electroluminescent Polymers

Electroluminescence (EL), light-emission upon electrical excitation, of conjugated polymers was first reported in 1990 [5], when J. H. Burroughes and coworkers noticed that the injection of an electron and a hole into the conjugated chain of polymers can lead to a self-localized excited state which can then decay radiatively, suggesting the possibility of using these materials in electroluminescent devices.

EL efficiency is defined as the number of photons emitted per electron injected. In devices which are intended to maximize the photonic output and efficiency such as LEDs, employing additional layers of organic polymers can promote the passage of electrons through the layer, and at the same time, provide a barrier to the passage of holes to significantly boost the electron injection, and hence improve the efficiency of the device [6]. In fact, the first diodes, consisting of only an insoluble polymer such as poly(1,4-phenylene vinylene) (PVV), sandwiched between a transparent anode and an aluminium cathode were not very efficient at converting the charges into light [5]. A later study by N. C. Greenham and coworkers has shown that it is possible to achieve improved efficiency in PVV LEDs by incorporating an electron-transporting layer (ETL) [7]. Other groups have demonstrated that the efficiency of LEDs can be further enhanced with the use of a hole-transporting layer (HTL) in conjugated polymers [8, 9]. Since 1990 electroluminescent polymers have experienced

an explosive growth in the research community worldwide. For example, in 1997 and 1998 Japanese groups designed three-layer polymer LEDs (PLEDs) which emit three different colors [10, 11].

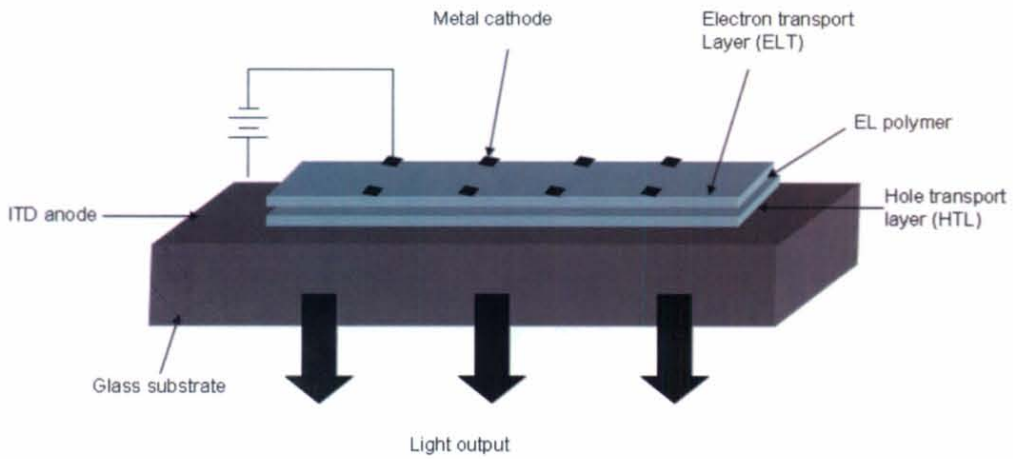

Figure 1.1: Typical design of an PLED showing optional electron and hole transport layers [12].

As shown in Fig. 1.1, a basic light-emitting device consists of ETL, HTL, and EL layer (often the same polymer is used for both the EL layer and ETL or HTL making the LED a two layered structure instead of three or more). These thin-film structures of layers are typically of the order of 100 nm thick. In addition, the device contains an optically transparent anode and a metallic cathode, together with a DC or AC power source. The anode is most often indium/tin oxide (ITO), while the cathode is a metal, such as Ca, Mg or Al. The conducting polymer is deposited on the ITO by spin-coating (a procedure that involves the application of a uniform thin film to a flat substrate) in solution. Materials used for ETL are electron deficient such as oxadiazole based compounds, and HTL are electron-accepting and are polymers such

as poly(vinyl carbazole). EL occurs when a singlet exciton, a coulombic bounded combination of electron and hole, decays to the ground state of the molecule [12].

In general, EL spectra and performance (i.e. color, efficiency, brightness, etc.) of PLEDs can be controlled by several factors such as the applied electric field, solvent, concentration of the solution used for spin casting (it is a commonly used technique for obtaining uniform thin film), and thickness of the film [13]. Solvent as one of the factors that affect the performance of PLEDs has been paid much attention to these days. For example, a California group [14] has reported that by using a proper solvent they could control the aggregation of polymer chains, and consequently, the emission color of the PLED. In addition, different kinds of solvents have various effects on PLEDs fabrication and their subsequent performance. PLEDs devices which are fabricated using nonaromatic solvents, such as tetrahydrofuran, have poorer polymer/anode contact and lower electrical conduction than those devices fabricated using aromatic solvents, such as dichlorobenzene [15]. There are many studies that have investigated the effects of a solvent on the performance of PLEDs (see for example the references [16, 17, 18]). As we can see from this brief discussion of PLEDs, an appropriate choice of a solvent can have enhancing effect on the performance of PLEDs.

As a part of this thesis, we are aiming to theoretically investigate the solvent effect on the electronic structure and energy of some conjugated polymers which have been shown to be promising candidates for PLEDs and/or organic solar cells. The systems that we investigate are polyfluorenes which are well known to emit blue light [19, 20, 21] and polycarbazoles which have been shown to be good electron donors in solar cells and possess outstanding electrical and photoelectrical properties [22, 23, 24, 25].

1.1.2 Polymer Solar Cells

The global energy demand is expected to be double in the next 50 years. Fossil fuels and biomass are responsible for the increased concentration of carbon dioxide in the Earth's atmosphere. Hence, developing environmentally friendly renewable energy source is one of the challenges in the 21^{st} century. One way to produce renewable and clean energy is to use photovoltaic (PV) devices that convert daylight into electricity.

Currently, the materials used to fabricate solar cells are mainly inorganic [26] such as silicon (Si), galluim-arsenide (GaAs), cadmium-telluride (CaTe) and cadmium-indium-selenide (CIS). Typically the power conversion efficiency (PCE) of these solar cells varies from approximately 10 to 30% [26]. The high cost of the production of silicon solar cells is one of the major obstacles that prevents these cells from providing large part of our electricity. That is the main reason why attention was directed to look for another kind of cheaper materials for commercialization purposes. Nowadays, many researchers have been looking for improving the efficiency of solar cells made entirely from organic materials, conjugated polymers and molecules [27, 28, 29, 30, 31]. It is hoped that in the future, these organic PV cells could provide electricity at lower cost than silicon PV solar cells.

Polymeric solar cells have emerged as a promising alternative for producing clean and renewable energy. They are environmentally safe, flexible, lightweight, and inexpensive. The cost reduction of polymeric solar cells is due to many reasons, the main one is due to ease of processability (polymers being soluble in various solvents) [26]. Most polymers such as PPV are not very soluble, however the attachment of side groups (such as alkyl chains) to the conjugated backbone significantly enhances the solubility of the polymer [32].

Generally, in solar cells there are four main processes that have to be optimized

in order to obtain a high power conversion efficiency (PCE) (see Fig. 1.2). The four processes are absorption of light, charge transfer and separation of different charges, charge transport, and charge collection at electrodes.

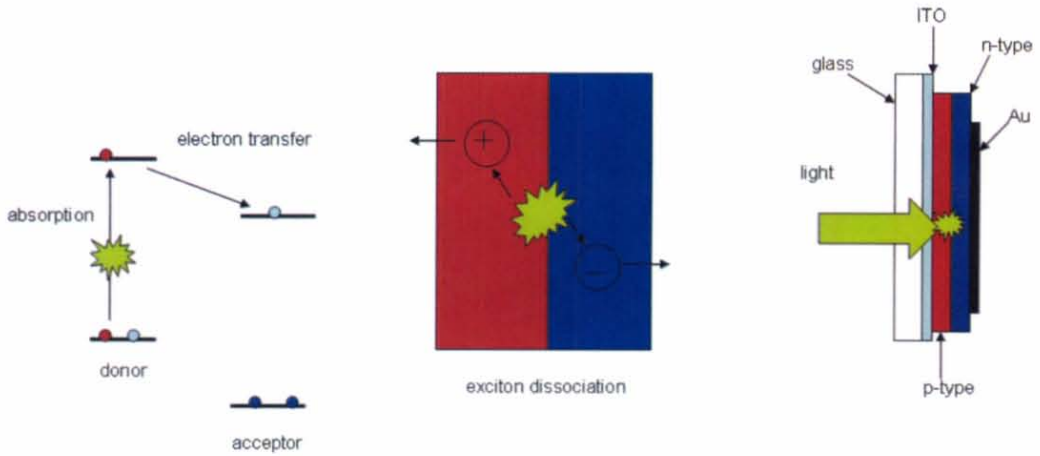

Figure 1.2: Schematic drawing of the working principle of an organic photovoltaic cell [26].

Photovoltaic cells based on organic materials are different from those based on inorganic materials, inorganic semiconductors generally have high dielectric constant and low exciton energy. Hence, the thermal energy at room temperature, k_BT = 0.025 eV, is enough to dissociate the exciton into a positive and negative charge carriers. In contrast, organic semiconductors have a lower dielectric constant and larger exciton binding energy. That is, exciton dissociation into free charge carriers does not occur at room temperature. Charges are then created by photoinduced electron transfer (an electron transfer when certain photoactive materials interact with light) [26].

The performance of a photovoltaic cell is characterized by the the power conversion

efficiency η_e (also referred to as PCE) which is given by:

$$\eta_e = I_{sc} V_{oc} FF, \tag{1.1}$$

where I_{sc} is the short-circuit current, V_{oc} is the open-circuit voltage and FF is the fill factor which is defined as the ratio of the maximum power from the solar cell to the product of V_{oc} and I_{sc}:

$$FF \equiv \frac{V_{MPP} \times I_{MPP}}{V_{oc} \times I_{sc}}, \tag{1.2}$$

where the subscript MPP denotes the maximum power point. Larger values of these parameters lead to higher η_e. That is, increasing the efficiency of solar cells requires implementing the fabrication procedures that influence I_{sc} and FF for a specific donor-acceptor system, and V_{oc} is obtained from the energy level difference between the component materials of the cell [28].

The ideal characteristics of the polymer (which is often used as a donor in bulk-hererojunction (BHJ) solar cells) are: the highest occupied molecular orbital (HOMO) is about -5.4 eV in order to obtain a high open-circuit voltage V_{oc} whose upper limit is often related to the energy difference between the HOMO of an electron donor and lowest unoccupied molecular orbital (LUMO) of an electron acceptor, hence the need for low HOMO of a donor; and the LUMO is about -4 eV in order to obtain a low band gap polymer. That is, for the optimal solar cell performance the ideal band gap of the polymer should be 1.5 eV. Also a high charge carrier mobility of about 10^{-1} $\mathrm{cm^2V^{-1}s^{-1}}$ is preferable for such an ideal donor to achieve a high PCE [33] (more realistically, this requirement is that the charge mobility be greater than 10^{-3} $\mathrm{cm^2V^{-1}s^{-1}}$).

Solution-processed BHJ photovoltaic cells which are polymer-fullerene composite

solar cells were first reported in 1995 [34]. Since that time, the number of publications on organic semiconductor photovoltaics has noticeably increased [35, 36, 37, 38]. The combination of poly(3-hexylthiophene) (P3HT) and [6,6]-phenyl-C_{61}-butyric acid methyl ester ($PC_{61}BM$) is still of great interest in the academic and industrial research areas, since its reported PCE is about 5% [28, 39]. However, in a very recent study, a higher PCE of about 7.4% was achieved in BHJ solar cells with the combination of poly[[4,8-bis[(2-ethylhexyl) oxy]-benzo[1,2-b:4,5-b']-dithiophene-2,6-diyl][3-fluoro-2-[(2-ethylhexyl)carbonyl]thieno[3,4-b]thio-phenediyl]] (PTB7) and $PC_{71}BM$. This high efficiency was achieved when the PTB7/$PC_{71}BM$ blend film was prepared from mixed solvent of chlorobenzene (CB)/1,8-diiodooctane (DIO) [40].

From the above brief discussion of solar cells (and PLEDs), it is clear that a solvent can play an important role in enhancing the PCE of solar cells. For this reason, we would like to investigate the solvent effect on ground state structure and dipole moments, and electronic energies of some conjugated polymers like PTB7 and another polymer called poly[4,8-dialkylbenzo[1,2-b:4,5-b']dithiophene-4,7-di(2-thienyl)-2,1,3-benzothiadiazole] (PBnDT-DTBT) [41] that have been shown to be good candidates for electron donors in BHJ solar cells. Furthermore, understanding the dynamic properties of conjugated polymers such as charge and energy transport can give a better idea on how to improve the performance of PLEDs and PVs. As a small contribution of this thesis, we investigated the solvent effect on the reorganization energy for the above mentioned polymers.

1.2 Current Research

In this thesis, using computational means, we investigate the solvent effect on the electron structure, energy, and charge transport properties of some conjugated polymers,

polyfluorenes (PF), polycarbazoles (PC), PTB7, and PBnDT-DTBT which have been proposed as good polymer candidates for PLED or BHJ solar cells. In all of our calculations, we used density functional theory (DFT) to determined their ground state properties. The excited states were calculated by using time-dependant DFT (TD-DFT). The solvent effect was studied with use of polarizable continuum solvation model (PCM). The exchange-correlation functional B3LYP with the polarized split-valence basis set, 6-31G^*, was employed in all the calculations. As mentioned above, the reason why we study the solvent effect is because it is evident that from recent interest in LEDs and PVs that the solvent can play important role in the performance of theses devices.

Generally, solvents can be classified into two categories, polar and non-polar. Solvent polarity has been defined and measured in several ways, one of the most common being the dielectric constant ϵ (also referred to as relative dielectric constant, static dielectric constant or static relative permittivity). Solvents with a dielectric constant of less than 15 are considered to be non-polar. High dielectric constant solvents ($\epsilon > 25$) usually have polar functional groups, and often high dipole moments. Physically, the dielectric constant of a solvent is related to the solvent's ability to reduce the solute's internal charge (that is, ϵ is related to the solvent's ability to reduce the strength of the electric field of charged solute particles relative to the strength of the electric field of these particles in a vacuum). The dielectric constant of a material is determined experimentally as the ratio of the capacitance of a capacitor using that material as a dielectric and the capacitance of a similar capacitor which has a vacuum as its dielectric [42].

The outline of the thesis as follows: Chapter 2 introduces the general theories of DFT, TD-DFT, PCM model and Marcus-Hush theory. The basic concepts of the exchange-correlation functionals, basis sets are also introduced. Chapter 3 gives a

summary of the computational details. Chapter 4 discusses the results obtained for fluorene and carbazole oligomers in the gas phase and in chloroform and methanol as solvents. Chapters 5 and 6 discuss the effect of a solvent on the electronic structure and energy, and some charge transport properties (hole-reorganization energy) of PTB7 and PBnDT-DTBT monomers. Chapter 7 summarizes the main conclusions of this thesis.

Chapter 2

Theoretical Approaches

In this chapter, we briefly summarize the theoretical approaches used in this thesis. We review density-functional theory (DFT) and time-dependant density-functional theory (TD-DFT) which are employed for atomic and molecular systems. Since the main aim of the thesis is to investigate the electronic structure of conjugated polymers in solution we also briefly discuss the theory of the solvation models such as polarizable continuum model (PCM) which we are using to study the solvent effect on the electronic structure of conjugated polymers.

2.1 DFT Method

During the past thirty years DFT has been the preferred theory for the electronic structure calculation in condensed matter physics. DFT is one of the post Hartree Fock (HF) approaches that includes the electron correlations beyond the HF approximation. The main difference between DFT and other molecular orbital theories such as HF is that the fundamental variable in DFT is the electron density ($\rho = \Psi^*\Psi$) rather than the electronic wave function Ψ [43].

2.1.1 Hohenberg-Kohn Theorems

In the mid 1960's W. Kohn and P. Hohenberg laid the foundation of today's DFT by showing that the electron density ρ could be used as a fundamental quantity to develop the many-body theory [44]. The first Hohenberg-Kohn theorem states that each external potential, $V_{ext}(\vec{r})$ (to within a constant) corresponds to a unique $\rho(\vec{r})$, that is, given $V_{ext}(\vec{r})$ which determines the Hamiltonain $\hat{H}$, the many particle ground state exists and is a unique functional of $\rho(\vec{r})$ such that

$$E_0 = E(\rho_0) \tag{2.1}$$

where E_0 is the ground state energy of a solid-state system. The exact form of the ground state energy function is not known.

The second Hohenberg-Kohn theorem uses the variational principle and says that any trial density $\rho(\vec{r})$ which satisfies the boundary conditions $\rho(\vec{r}) \geq 0$ and $\int \rho(\vec{r})d\vec{r} = N$, and is associated with V_{ext}, represents an upper bound to the ground state energy, that is,

$$E_0 \leq E(\rho) \tag{2.2}$$

where $E(\rho)$ is the electronic energy of the system [44].

2.1.2 Kohn-Sham Equations

The many-body time-independent Schrödinger equation for the electrons has the following form:

$$\hat{H}\Psi = [\hat{T} + \hat{V} + \hat{V}_{ee}]\Psi = [\sum_{i}^{N} \frac{-\hbar^2}{2m}\nabla_i^2 + \sum_{i}^{N} V(\vec{r_i}) + \sum_{i<j}^{N} V_{ee}(\vec{r_i}, \vec{r_j})]\Psi = E\Psi \tag{2.3}$$

where $\hat{T}$ is the electron kinetic energy operator, $\hat{V}$ is the potential energy operator due to electron-nucleus interactions and corresponds to V_{ext} (see Section 2.1.1), $\hat{V}_{ee}$ is the potential energy operator due to electron-electron interactions, and Ψ is the total electronic wave function. In DFT, the electronic energy (expectation value of the above Hamiltonian) becomes a functional of density ρ as follows,

$$E = E[\rho] = \langle \Psi[\rho] | \hat{T} + \hat{V} + \hat{V}_{ee} | \Psi[\rho] \rangle \tag{2.4}$$

or

$$E = \langle T[\rho] \rangle + \langle V_{ee}[\rho] \rangle + \int V(\vec{r}) \rho(\vec{r}) d\vec{r}. \tag{2.5}$$

The exchange-correlation energy functional E_{xc} is defined by the sum of the kinetic energy deviation from the reference system and the electron-electron repulsion energy deviation from the classical system,

$$E_{xc}[\rho] = \Delta \langle T[\rho] \rangle + \Delta \langle V_{ee}[\rho] \rangle. \tag{2.6}$$

The functional form of the E_{xc} is not known [45]. Applying the variational principle and the condition $\langle \phi_i | \phi_j \rangle = \delta_{ij}$ [44] where ϕ_i and ϕ_j are single electron spin orbitals, the Kohn-Sham equations can be obtained and solved in a self consistent way as follows,

$$[-\frac{1}{2}\nabla^2 + V_{eff}(\vec{r})]\phi_i = \varepsilon_i \phi_i. \tag{2.7}$$

In Eq. (2.7) the effective potential $V_{eff}(\vec{r})$ can be written as

$$V_{eff}(\vec{r}) = V_C + V_{xc}(\vec{r}) = V(\vec{r}) + \int \frac{\rho(\vec{r_i})}{|\vec{r_j} - \vec{r_i}|} d\vec{r_i} + \frac{\delta E_{xc}}{\delta \rho(\vec{r})}, \tag{2.8}$$

where the exchange-correlation potential V_{xc} is the functional derivative of exchange-correlation energy functional E_{xc},

$$V_{xc}(\vec{r}) \equiv \frac{\delta E_{xc}}{\delta \rho(\vec{r})}, \tag{2.9}$$

and V_C (where C stands for Coulomb) is the term includes the first and second terms in the right hand side of Eq. (2.8). The minimized ϕ_i in Eq. (2.7) is used to calculate the ground state density ρ_0 and the energy E_0.

2.1.3 The Exchange-Correlation Energy Functionals

Since the exact functional form of E_{xc} is not known, we need good approximations of E_{xc} in order to make practical use of DFT. The simplest and most widely used approximation for E_{xc} is the local density approximation (LDA); magnetic and open-shell systems are better described by the local spin density approximation (LSDA). The second level of approximation is the so-called generalized gradient approximation (GGA) [46]. Most recently, hybrid functionals have become widely used [47].

In general, the exchange-correlation energy term can be written as a sum of correlation and exchange terms as follows

$$E_{xc} = E_x + E_c. \tag{2.10}$$

In the local density approximation (LDA), E_{xc} is given by

$$E_{xc}^{LDA}[\rho] \equiv \int \epsilon_{xc}[\rho]\rho(\vec{r})d\vec{r}, \tag{2.11}$$

where ϵ_{xc} is the exchange-correlation energy per particle of a uniform interacting

electron gas of density $\rho(\vec{r})$. In the generalized gradient approximation (GGA) E_{xc} is written in the form

$$E_{xc}^{GGA} \equiv \int f(\rho(\vec{r}), |\Delta\rho(\vec{r})|)d\vec{r} \tag{2.12}$$

where $f(\rho, |\Delta\rho|)$ is a suitably chosen function of the two variables [46]. The LDA and GGA do not reproduce the exchange energy as in the HF. Another approximation which combines DFT correlation and exchange that is a combination of the DFT and HF contributions gives rise to so-called hybrid functionals of the following general form [43],

$$E_{xc}^{hyp} = \alpha E_x^{HF} + (1-\alpha)E_x^{DFT} + E_c^{DFT} \tag{2.13}$$

where α is a fitted coefficient to some molecular properties (experimentally determined). These hybrid functionals tend to give better results for the exchange and correlation. One example of an exchange-correlation functional as suggested and tested by Becke [49] has the form

$$E_{xc} = (1-a_0)E_x^{LSDA} + a_0 E_x^{HF} + a_x \Delta E_x^{B88} + E_c^{LSDA} + a_c \Delta E_c^{PW91} \tag{2.14}$$

where ΔE_x^{B88} is Becke's gradient correction to the exchange functional, ΔE_c^{PW91} is Perdew-Wang gradient correction to the local correlation functional [50], and the coefficients a_0, a_x and a_c have the values 0.2, 0.72 and 0.81 respectively, (these coefficients were based on fitting to heats of formation of small molecules [49]).

Another hybrid exchange-correlation functional was also suggested by Becke and is referred to as B3LYP [48]. B3LYP is one of the most accurate and widely used hybrid functionals today. This functional is used in this thesis. The B3LYP functional in Gaussian/DFT package uses the LYP functional for the correlation. Since LYP does not have an easily separable local component, the VWN local correlation has

been used to give the different coefficients of local and gradient corrected correlation functionals [49] as follows:

$$E_{xc}^{\text{B3LYP}} = (1-a_0)E_x^{LSDA} + a_0E_x^{HF} + a_x\Delta E_x^{B88} + a_cE_c^{LYP} + (1-a_c)E_c^{VWN} \quad (2.15)$$

where E_c^{VWN} is the Vosko-Wilk-Nusiar correlation functional [51] and E_c^{LYP} is the correlation functional due to Lee, Yang, and Parr [52]. The explicit form of B3LYP functional as defined in Gaussian users manual [53, 54] has the form

$$\text{B3LYP} = 0.2 * XHF + 0.8 * XS + 0.72 * XB88 + 0.19 * VWN + 0.81 * LYP \quad (2.16)$$

XHF denotes HF exchange, XS denotes Dirac-Slater exchange and the other terms are defined above.

2.1.4 Basis Set

In the beginning of 1950's, Roothaan pointed out that molecular orbitals (MO's) can be expressed as a linear combination of a basis functions, usually referred to as a linear combination of atomic orbitals (LCAO) [55]. These basis functions are often centered on the atomic nuclei. An individual molecular orbital is defined as

$$\phi_i = \sum_{\mu=1}^{N} c_{\mu i}\chi_\mu \quad (2.17)$$

where the coefficients $c_{\mu i}$ are known as the molecular orbital expansion coefficients. The basis functions $\chi_1 ... \chi_N$ are normalized and expressed in terms of primitive basis functions g's. The most used basis functions are Slater-type or Gaussian-type functions. In this thesis we use in all DFT, TD-DFT, and solvation calculations

Gaussian-type basis functions. Gaussian 03, Gaussian 09, and other ab initio electronic structure programs use Gaussian-type atomic functions as basis sets, which are linear combinations of primitive gaussian functions of the general form

$$g(\alpha, \vec{r}) = cx^n y^m z^l e^{-\alpha r^2} \tag{2.18}$$

α is a constant that determines the size (radial extent) of the function [56]. Gaussian-type basis sets are often used in ab initio calculations because they are easier than Slater-type to deal with in the many numerical integrations that are performed in the self-consistent field calculations. In this thesis the polarized split-valence basis set 6-31G^* is used for all calculations, which contains 6 gaussian primitives for each inner-shell function, and splits the valence orbitals into two contractions with 3 and 1 gaussian primitives in each, and the asterisk indicates the addition of the six d-type primitives to 6-31G basis set to take into account the polarization effect.

2.2 TD-DFT

A time dependent formalism of DFT has opened the way to the computation of excited energies and frequency dependent response functions such as the dynamic polarizability. The foundation of TD-DFT was laid by Runge and Gross in 1984 [57] when they derived a Hohenberg-Kohn-like theorem for the time-dependent Schrödinger equation (TD-SE).

2.2.1 Runge-Gross Theorem

The Runge-Gross theorem considers a single-particle system in the presence of a time dependent field. The Hamiltonian can be written as:

$$\hat{H}(t) = \hat{T} + \hat{V}_{ext}(t) + \hat{V}_{ee} \tag{2.19}$$

where $\hat{T}$ is the kinetic energy operator, $\hat{V}_{ext}$ is the external potential operator, and $\hat{V}_{ee}$ is the electron-electron interaction operator. For more details about the explicit forms of these operators the reader is referred to Ref. [57]. The starting point is the TD-SE

$$\hat{H}(t)\phi(t) = i\frac{\partial\phi(t)}{\partial t}, \quad \phi(t_0) = \phi_0. \tag{2.20}$$

The theorem states that no two external potentials, $V_1(\vec{r}, t)$ and $V_2(\vec{r}, t)$, which differ by more than time-dependent function $c(t)$, can produce the same time-dependent density $\rho(\vec{r}, t)$. The proof of this theorem is in two steps: first, it is shown that the current densities, j_1 and j_2, generated by V_1 and V_2 (such that $V_1(\vec{r}, t) \neq V_2(\vec{r}, t)+c(t)$), are also different. Second, by the use of the equation of continuity, if it is pointed out that the two systems have different current densities, they must also have different time-dependent electron densities. i.e., $j_1 \neq j_2$ implies that $\rho_1(t) \neq \rho_2(t)$. It should be mentioned that the two current densities are identical at the initial time t_0, since the initial wave function ϕ_0 is fixed, and the external potential is expanded in Taylor expansion around t_0 [57, 58].

2.2.2 Time-Dependent Kohn-Sham equations

After demonstrating the Runge-Gross theorem which shows that a given external interaction potential can determine the density uniquely, it is possible to construct a time-dependent Kohn-Sham scheme. The Kohn-Sham Hamiltonian is defined as

$$\hat{H}_{KS}(\vec{r}, t) \equiv -\frac{\nabla^2}{2} + V_{KS}[\rho](\vec{r}, t) \tag{2.21}$$

where $V_{KS}[\rho](\vec{r},t)$ is the time-dependent Kohn-Sham potential which normally is written as

$$V_{KS}[\rho](\vec{r},t) = V_{ext}(\vec{r},t) + V_{ee}[\rho](\vec{r},t) + V_{xc}[\rho](\vec{r},t). \tag{2.22}$$

$V_{ext}(\vec{r},t)$ is the external potential, $V_{ee}[\rho](\vec{r},t)$ is the electrostatic interaction which is given by the following equation

$$V_{ee}[\rho](\vec{r},t) = \int d^3r' \frac{\rho(\vec{r'},t)}{\mid \vec{r} - \vec{r'} \mid}. \tag{2.23}$$

The time-dependent density can be calculated from the Kohn-Sham orbitals [58] as

$$\rho(\vec{r},t) = \sum_{i}^{N} \mid \phi_i(\vec{r},t) \mid^2 . \tag{2.24}$$

$V_{xc}[\rho](\vec{r},t)$ is the exchange-correlation potential which has a complex functional dependence on the density.

In fact, in the time-dependent system the total energy is not minimized. However, there is a quantity called the quantum mechanical action integral given by the form

$$A[\Psi] = \int_{t_0}^{t_1} dt < \Psi(t) \mid i\frac{\partial}{\partial t} - \hat{H}(t) \mid \Psi(t) > \tag{2.25}$$

where $\Psi(t)$ is an N-body wave function which is minimized. So far, the TD-Kohn-Sham equations are restricted for two cases: (i) if the external potential is a periodic function of time, this can be proved with the *adiabatic approximation* to ground state energy [59]; and (ii) for the potential containing small perturbations, this can be solved by linear-response theory [60].

By using the Keldysh formalism of complex-time path integration [61], and introducing a new action function $A[\rho]$ that does not explicitly depend on $\frac{\partial}{\partial t}$, it is possible

to write the quantum action integral as

$$A[\rho] = A_{KS}[\rho] - A_{xc}[\rho] - \frac{1}{2}\int_{\tau_0}^{\tau_1} d\tau \dot{t}(\tau) \int d^3r \int d^3r' \frac{\rho(\vec{r},\tau)\rho(\vec{r'},\tau)}{|\vec{r}-\vec{r'}|} \tag{2.26}$$

where $A_{KS}[\rho]$ is the Kohn-Sham quantum action, τ is Keldysh pseudotime, $\dot{t}$ is shorthand for $dt/d\tau$ and $A_{xc}[\rho]$ is the exchange-correlation quantum action, so that the exchange-correlation potential is given by

$$V_{xc}(\vec{r},t) = \frac{\delta A_{xc}[\rho]}{\delta\rho(\vec{r},\tau)} \mid_{\rho=\rho(\vec{r},t)} \tag{2.27}$$

which is similar to the time-independent DFT equation.

2.2.3 Linear Response TD-DFT

Linear response TD-DFT can be used if the external perturbation is small in the sense that does not significantly change the ground state structure of the system. This means that the variation of the system will depend only on the ground state wave function so that we can use the properties of ground state DFT [58].

Consider a small time-dependent external perturbation $\delta V_{ext}(t)$. We can write the Hamiltonian in the form

$$H'(t) = H + \delta V_{ext}(t). \tag{2.28}$$

Also we can write the Kohn-Sham Hamiltonian (see Eq. (2.22)) as

$$H'_{KS}[\rho](t) = H_{KS}[\rho] + \delta V_{ee}[\rho](t) + \delta V_{xc}[\rho](t) + \delta V_{ext}(t). \tag{2.29}$$

To linear order we can write the time-dependant density for the Hamiltonian in Eq.

(2.28) as

$$\delta\rho(\vec{r},t) = \chi(\vec{r}t,\vec{r'}t')\delta V_{ext}(\vec{r'}t'), \tag{2.30}$$

and Kohn-Sham time-dependant density as

$$\delta\rho(\vec{r},t) = \chi_{KS}(\vec{r}t,\vec{r'}t')\delta V_{eff}[\rho](\vec{r'}t'), \tag{2.31}$$

where $\delta V_{eff}[\rho](t) = \delta V_{ext}(t) + \delta V_{ee}[\rho](t) + \delta V_{xc}[\rho](t)$ and the primed variables are integrated. Within the linear-response domain, the variation of V_{ee} and V_{xc} to linear order may be expanded with respect to the density variation as

$$\delta V_{ee}[\rho](\vec{r}) = \frac{\delta V_{ee}[\rho]}{\delta\rho}\delta\rho = \frac{1}{\mid \vec{r} - \vec{r'} \mid}\delta\rho(\vec{r'}) \tag{2.32}$$

and

$$\delta V_{xc}[\rho](\vec{r}) = \frac{\delta V_{xc}[\rho]}{\delta\rho}\delta\rho = f_{xc}(\vec{r}t,\vec{r'}t')\delta\rho(\vec{r'}). \tag{2.33}$$

Then, by inserting the last two equations in the response equation for the KS system we get

$$\chi(\vec{r_1}t_1,\vec{r_2}t_2) = \chi_{KS}(\vec{r_1}t_1,\vec{r_2}t_2) + \chi_{KS}(\vec{r_1}t_1,\vec{r_2'}t_2')\left(\frac{1}{\mid \vec{r_2'} - \vec{r_1'} \mid} + f_{xc}(\vec{r_2'}t_2',\vec{r_1'}t_1')\right)\chi(\vec{r_1'}t_1',\vec{r_2'}t_2'). \tag{2.34}$$

From the last equation we can obtain the excitation energies of the system, as they are the poles of the response function (for further discussion see Ref. [58]).

2.3 Solvation Models

In the last century, many different approaches and theoretical models aimed at describing the effects of surrounding environment on the properties of selected system.

The effect of the surrounding environment is called solvation or embedding [62]. One way of modeling systems in non-aqueous solution is Self-Consistent Reaction Field (SCRF). This method models the solvent as a continuum of a uniform dielectric constant ϵ. The solute is placed into a cavity within the solvent. There are four different SCRF models, which differ in how the cavity and the reaction field are defined [56]. These models are the Onsager reaction field model, Tomasi's Polarized Continuum Model (PCM), the Isodensity Polarized Continuum Model (IPCM) and the Self-Consistent Isodensity Polarized Continuum Model (SCI-PCM). The limitation of the Onsager model is that it treats the the systems with zero dipole moment as in the gas phase. The best model is SCI-PCM, but it is computationally very expensive.

The polarizable continuum model (PCM), which we mainly used in this work, is used for the calculations of molecular energies, structure, and properties in liquid solution in HF and DFT approaches at a reasonable computational cost. The PCM defines the cavities as envelopes of spheres centered on atoms or atomic groups [63].

2.3.1 PCM Model

The most recent version of PCM model has been derived in two different ways; the first one is called integral equation formalism (IEF-PCM) [64] and the second is implicit volume charges (IVC-PCM) [65]. The IEF-PCM method has been derived first and can be applied to isotropic and anisotropic solvents and also to ionic solutions [66]. This common formulation (also simply called PCM) is presented in *GAUSSIAN* packages [53]. In the rest of this section we are going to discuss briefly the theory behind IEF-PCM method (or simply PCM).

Consider two charge distributions, ρ and ρ', carried by the solute molecule and

located inside the cavity Ω_i. The electrostatic interaction energy is given by

$$E_I(\rho, \rho') = \int_{R^3} \rho'(x) V(x) dx, \tag{2.35}$$

where $V(x)$ is the electrostatic potential created by the presence of ρ and satisfies the Poisson equation,

$$-\mathsf{div}(\epsilon(x) \cdot \nabla V(x)) = \rho(x) \tag{2.36}$$

where

$$\epsilon(x) = \left\{ \begin{array}{ll} \epsilon_i & \text{if } x \in \Omega_i \\ \epsilon_e & \text{if } x \in \Omega_e \end{array} \right\}, \tag{2.37}$$

ϵ_i is the unit 3x3 tensor , ϵ_e is a positive 3x3 symmetric tensor and Ω_e is the outer domain of the cavity. The notation used in this Section is the same as in Ref. [64]. It should be noted that Eq. (2.35) is a 3D integral. By choosing orthonormal coordinates of real space ϵ_e can be made diagonal [64],

$$\epsilon_i = \begin{pmatrix} 1 & 0 & 0 \\ 0 & 1 & 0 \\ 0 & 0 & 1 \end{pmatrix}, \quad \epsilon_e = \begin{pmatrix} \epsilon_1 & 0 & 0 \\ 0 & \epsilon_2 & 0 \\ 0 & 0 & \epsilon_3 \end{pmatrix}. \tag{2.38}$$

Next define G_i as the Green's function of the operator $-\Delta$ and G_e as the Green's function of the operator $-\mathsf{div}(\epsilon \cdot \nabla V)$, so we can define the function

$$G(x,y) = \left\{ \begin{array}{ll} G_i(x,y) = \frac{1}{4\pi|x-y|} & \text{if } x \in \Omega_i \\ G_e(x,y) = \frac{1}{4\pi\sqrt{\mathsf{det}[\,\epsilon_e(\epsilon_e^{-1}\cdot(x-y))\cdot(x-y)]}} & \text{if } x \in \Omega_e \end{array} \right. . \tag{2.39}$$

Then by defining the operators of Calderon projector [67] for the above Green func-

tions we obtain:

$$\begin{aligned}(S_i.u)(x) &= \int_\Gamma G_i(x,y)u(y)dy \\ (D_i.u)(x) &= \int_\Gamma \partial_y G_i(x,y)u(y)dy \\ (D_i^*.u)(x) &= \int_\Gamma \partial_x G_i(x,y)u(y)dy\end{aligned} \tag{2.40}$$

where Γ is the cavity boundary, $\partial_y G(x,y) = \nabla_y G_i(x,y)\cdot n(y)$, $\partial_x G(x,y) = \nabla_x G_i(x,y)\cdot n(x)$, $n(x)$ and $n(y)$ are the normals pointing outward at x and y respectively, $u(x) \in L^2(\Gamma)$ and $x \in \Gamma$. L^2 is the area of tesserae (small surface area). S_i is a self-adjoint operator (defined below) and D_i^* is the adjoint of D_i. The operator D_i is related to the electric field created by the surface charge σ, and it is also defined below. It can be proved that $S_i D_i^* = D_i S_i$. The same procedures can be done for the function G_e defined in the outer space of the cavity [64]. Introducing the electrostatic potential $\phi'(x)$ generated by the charge density ρ' in the vacuum, and the function $f(x)$ such as

$$\phi'(x) = \int_{R^3} G_i(x,y)\rho'(y)dy, \quad f(x) = \int_{R^3} G(x,y)\rho(y)dy \tag{2.41}$$

we can define an apparent potential $W = V - f$ and rewrite the interaction energy of Eq. (2.35) as

$$E_I(\rho,\rho') = E_1 + E_2 = \int_{R^3} \rho'(x)f(x)dx + \int_{R^3} \rho'(x)W(x)dx. \tag{2.42}$$

E_1 is easy to compute since it is supposed that both charge distributions are inside Ω_i. The detailed discussion of how to simplify E_2 by introducing the quantity $\sigma = S_i^{-1}\cdot W_i$, which has the dimension of a surface charge, is given in Ref. [64]. Following this discussion E_2 can be written as

$$E_2 = \int_\Gamma \sigma(x)\phi_i'(x)dx. \tag{2.43}$$

where ϕ_i' is the electrostatic potential generated by the charge density ρ' inside the cavity. After calculating the electrostatic energy, the equivalent surface charge σ in Eq. (2.43) is given by

$$A \cdot \sigma = g \tag{2.44}$$

where

$$A = (\frac{I}{2} - D_e)S_i + S_e(\frac{I}{2} + D_i^*) \tag{2.45}$$

and

$$g = -(\frac{I}{2} - D_e)f_i - S_e \cdot \partial f_i, \tag{2.46}$$

where I is the identity matrix. For more details about the proof of Eq. (2.44) the reader is referred to Ref. [68]. It should be mentioned that when ϵ_e is scalar (i.e. the dielectric is isotropic), we have $S_e = S_i/\epsilon_e$, $f_e = f_i$, and $D_e = D_i$. Denoting $\partial f_i = -E_n$, where E_n is the normal component of the electric field at point x generated by the surface charge σ which is given by

$$E_n(\vec{x}) = D^*\sigma(\vec{x}) - 2\pi\sigma(\vec{x}) \tag{2.47}$$

where the operator $D\sigma(x)$ (is related to the overall flux of the electric field due to $\sigma(\vec{x})$) has the form

$$D\sigma(\vec{x}) = \int_{\Gamma-\delta x} \sigma(\vec{x'}) \frac{(\vec{x} - \vec{x'}) \cdot \hat{n_{x'}}}{\mid x - x' \mid^3 d\vec{x'}}, \tag{2.48}$$

then by using the relation $(\frac{I}{2} - D_i) \cdot f_i + S_i \cdot \partial f_i = 0$ [64], Eq. (2.44) becomes

$$S_i \left[\left(\frac{I}{2} - D_i^* \right) + \frac{1}{a_e} \left(\frac{I}{2} + D_i^* \right) \right] \cdot \sigma = -\frac{\epsilon_e - 1}{\epsilon_e} S_i \cdot E_n \tag{2.49}$$

and after multiplication by $(\epsilon_e/\epsilon_e - 1)S_i^{-1}$, we get

$$\left(\frac{\epsilon_e + 1}{\epsilon_e - 1}\frac{I}{2} - D_i^*\right) \cdot \sigma = -E_n. \tag{2.50}$$

The last equation is exactly the operator-like form of the matrix equation for the standard PCM model. The polarization charge density depends on the electrostatic potential generated by the solute on the cavity [66], so the Eq. (2.50) becomes

$$\left[\frac{\epsilon_e + 1}{\epsilon_e - 1}S - \frac{1}{2\pi}SD^*\right]\sigma(\vec{x}) = \left[-1 + \frac{1}{2\pi}D\right]V(\vec{x}), \tag{2.51}$$

where $V(\vec{x})$ is the electronic and nuclear solute potential in point x on the cavity surface. S is an operator related to the the electrostatic potential due to the charge on the surface by the following equation [66]

$$S\rho(\vec{x}) = \int_{\Gamma - \delta x} \frac{\rho(\vec{x'})}{\mid x - x' \mid} d\vec{x'} + 1.0694\rho(\vec{x})\sqrt{4\pi a(\delta x)}, \tag{2.52}$$

where $a(\delta x)$ is the area of the region around x excluded from the integration.

In the computational work, the charge distribution on the surface $\sigma(\vec{x})$ is expressed in terms of a set of point charges located at the center of each tessera [66]. These charges are collected in the column vector $\mathbf{q}$, whose dimension is the number of surface tesserae N_{TS}. In Eq. (2.51) the operators are replaced by the corresponding N_{TS}xN_{TS} matrices $\mathbf{S}$,$\mathbf{D}^*$, and $\mathbf{D}$; the complete forms of the elements of these matrices are given in Ref. [66].

Thus, the PCM equations in quantum mechanical (QM) calculations are

$$\mathbf{Tq} = \mathbf{RV} \tag{2.53}$$

where

$$\mathbf{T} = \frac{\epsilon_e + 1}{\epsilon_e - 1}\mathbf{S} - \frac{1}{2\pi}\mathbf{DAS} \tag{2.54}$$

and

$$\mathbf{R} = -\mathbf{I} + \frac{1}{2\pi}\mathbf{DA}, \tag{2.55}$$

and in the molecular mechanical (MM) calculations

$$\left[2\pi\frac{\epsilon_e + 1}{\epsilon_e - 1}\mathbf{A}^{-1} - \mathbf{D}^*\right]\mathbf{q} = -\mathbf{E}_n \tag{2.56}$$

where $\mathbf{A}$ is a diagonal matrix containing the area of tesserae.

2.3.2 PCM Correction to the Hamiltonian

Once the solvation charges have been determined through Eq. (2.53) or Eq. (2.56) they can be used to compute energies and properties in solution. In molecular mechanics, the calculations of solvent effect on energies is straightforward, while in quantum mechanics calculations the molecular Hamiltonian must be corrected by a suitable PCM operator [66].

In the presence of a solvent the Hamiltonian has the following form:

$$\hat{H}^\circ\psi^\circ = E^\circ\psi^\circ \qquad \text{in vacuo,} \tag{2.57}$$

$$[\hat{H}^\circ + \hat{V}^\dagger]\psi = E\psi \qquad \text{in solution} \tag{2.58}$$

where $\hat{H}^\circ$ is the Hamiltonian of the solute in vacuo (including nuclear repulsion terms), ψ° and ψ are the solute wave functions in vacuo and in solution respectively, and $\hat{V}^\dagger$ is the solute-solvent interaction potential operator which acts as a perturbation on the solute Hamiltonian [64].

The interaction energy between the solute and the solvation charges can be written as:

$$E_{int} = \mathbf{V}^{\dagger}\mathbf{q} = \sum_{i} V_i q_i, \tag{2.59}$$

where V_i is the solute potential in tesserae i. Since the charges depend on σ through the potential, the solute density and charges must be adjusted until self-consistency is reached. In practice, this is done during the SCF procedure in HF or DFT calculations [66]. If $E^0 = E[\rho^0] + V_{NN}$ is the solute energy in vacuo, the free energy U minimized in solution is

$$U = E[\rho] + V_{NN} + \frac{1}{2}\mathbf{V}^{\dagger}\mathbf{q}, \tag{2.60}$$

where V_{NN} is the solute nuclear repulsion energy, ρ^0 is the electronic density for the isolated molecule, and ρ is the electronic density of the solute perturbed by the solvent. The above expression applies to HF as well as to DFT [66]. Eq. (2.60) can also be written as

$$U = E[\rho] + V_{NN} + \frac{1}{2}\mathbf{V}^{\dagger}\mathbf{Q}\mathbf{V}, \tag{2.61}$$

where

$$\mathbf{Q} = \mathbf{T}^{-1}\mathbf{R}. \tag{2.62}$$

It is clear that the PCM contribution can be expressed using a response matrix $\mathbf{Q}$ which connects the solute potential on different points on the surface. If we define the electronic density on a basis of atomic functions [66] as

$$\rho(\vec{r}) = \sum_{\mu\nu} P_{\mu\nu}\chi_{\mu}(\vec{r})\chi_{\nu}(\vec{r}), \tag{2.63}$$

where $\chi_{\mu}(\vec{r})$ and $\chi_{\nu}(\vec{r})$ are the atomic functions, and $P_{\mu\nu}$ is an element of the density

matrix, then one can define a Fock (or Kohn-Sham) matrix [66] with elements as

$$F_{\mu\nu} = \frac{\partial U}{\partial P_{\mu\nu}} = F^0_{\mu\nu} + v^{PCM}_{\mu\nu}. \tag{2.64}$$

$F^0_{\mu\nu}$ is an element of the Fock matrix for isolated molecule, and PCM matrix is written as

$$v^{PCM}_{\mu\nu} = \frac{1}{2}\mathbf{V}^{\dagger}_{\mu\nu}\mathbf{Q}\mathbf{V} + \frac{1}{2}\mathbf{V}^{\dagger}\mathbf{Q}\mathbf{V}_{\mu\nu} \tag{2.65}$$

where the potential in tesserae i is

$$V^i_{\mu\nu} = \int \chi_\mu(\vec{r}) \frac{1}{\mid \vec{r} - \vec{x_i} \mid} \chi_\nu(\vec{r}) d\vec{r}. \tag{2.66}$$

Since $\mathbf{Q}$ is not symmetric, the two term in the r.h.s. of Eq. (2.65) are not equal. However, the PCM term can be rearranged as follows:

$$\mathbf{V}^{\dagger}\mathbf{Q}\mathbf{V} = \sum_{ij} V_i Q_{ij} V_j = \frac{1}{2}[\sum_{ij} V_i Q_{ij} V_j + \sum_{ij} V_j Q_{ji} V_i] = \sum_{ij} V_i \frac{(Q_{ij} + Q_{ji})}{2} V_j. \tag{2.67}$$

Then we can use a symmetrized matrix $(\mathbf{Q} + \mathbf{Q}^{\dagger})/2$ to define

$$w_i = \sum_j \frac{(Q_{ij} + Q_{ji})}{2} V_j, \tag{2.68}$$

so that

$$v^{PCM}_{\mu\nu} = \mathbf{w}^{\dagger}\mathbf{V}_{\mu\nu} = \sum_i w_i V^i_{\mu\nu}. \tag{2.69}$$

It should be noted that there is a difference between the definitions of solvation charges $\mathbf{q} = \mathbf{Q}\mathbf{V}$ and the solvation weights $\mathbf{w} = [(\mathbf{Q} + \mathbf{Q}^{\dagger})/\mathbf{2}]\mathbf{V} = \mathbf{V}^{\dagger}[(\mathbf{Q} + \mathbf{Q}^{\dagger})/\mathbf{2}]$ [66] in the above formalism. Once the Fock (or Kohn-Sham) matrix is determined in the presence of a solvent, the standard quantum mechanical (SCF) methods are used to solve it

(i.e. obtain its eigenvalues and eigenvectors).

2.4 Charge Transfer Rates (Reorganization Energy)

For systems with weak intermolecular interactions, such as those considered in this thesis, bulk charge transport can be described by a hopping model such as that proposed by Marcus and Hush [69]. In the Marcus-Hush theory the charge transfer rate Γ_{ij} (between two sites on a given lattice) is given by

$$\Gamma_{ij} = \frac{t_{ij}^2}{\hbar}\sqrt{\frac{\pi}{\lambda\kappa_B T}}\exp\left\{-\frac{(\Delta G_{ij}-\lambda)^2}{4\lambda\kappa_B T}\right\} \tag{2.70}$$

where t_{ij} is the electronic transfer integral, λ is the molecular reorganization energy, and T is the temperature, and κ_B, $\hbar$, and ΔG_{ij} are the Boltzmann's constant, reduced Plank's constant, and the free energy difference between the initial and final sites respectively. In this thesis, we investigate the solvent effect on transport properties of conjugated polymers by calculating the hole reorganization energies for some systems. It is clear from the above equation that the smaller λ gives higher Γ_{ij} which in turn leads to better bulk charge transport.

2.4.1 Reorganization Energy

The hole and electron reorganization energies are important in calculating the transfer rates as is shown in Eq. (2.70). If the molecular vibrations and polarizations due to surrounding medium are neglected, then the reorganization energy for hole transport λ_h in the reaction that contains acceptor molecule (A) and donor molecule (D) and is given by $D + A^{\bullet+} \rightarrow D^{\bullet+} + A$ where D is neutral donor and $A^{\bullet+}$ is a radical cation can be determined as in [70] as follows: $\lambda_h = (E_{nuet}(D^{\bullet+}) - E_{opt}(D^{\bullet+})) + (E_{radc}(A) -$

$E_{opt}(A)$). $E_{nuet}(D^{\bullet+})$ is the energy of $D^{\bullet+}$ calculated at neutral cation geometry and $E_{opt}(D^{\bullet+})$ is the energy calculated at optimal cation geometry. $E_{radc}(A)$ and $E_{opt}(A)$ are the energies of A at radical cation and optimal ground state geometries respectively. In summary, the geometry is optimized for both the neutral and the radical cation states and the energies corresponding to the neutral and cationic electronic configurations are computed for each of the two optimized geometries. Thus, we calculate a set of four energies, corresponding to the neutral molecule at the neutral geometry, the cation at the neutral geometry, the neutral molecule at the cation geometry, and the cation at the cation geometry for each λ_h. The electron reorganization energy can be computed in similar way.

Chapter 3

Computational Details

All the calculations in this thesis have been performed with both Gaussian 03 (G03) [53] and Gaussian 09 (G09) [71] software packages, which are provided by the Atlantic Computational Excellence network (ACEnet). ACEnet machines support parallel jobs which can minimize our computational time. For F and C oligomers, it usually took from six hours to three days for each optimized calculations, while it took up to one or two weeks for the larger PTB7 and PBnDT-DTBT monomers.

We have performed DFT calculations to calculate the ground state properties in the gas phase and in solvents for all the systems investigated in the thesis: F and C oligomers, and PTB7 and PBnDT-DTBT monomers. As was discussed in Chapter 2, the B3LYP hybrid exchange-correlation functional was used for all the calculations. The polarized split-valence basis set, 6-31G^*, was employed; it is comprised of a linear combination of six gaussian primitives for the inner-shell functions, and three and one gaussian primitives for the two valence shells. The asterisk corresponds to d in gaussian packages [53], which indicates the addition of the six d-type primitives to 6-31G basis set to take into account the polarization effect [72].

All the systems studied in this work were geometry optimized by using the OPT

keyword in G03 and G09 input files. This keyword searches for the global minimum on the potential energy surface (PES) which occurs when the energy gradient with respect to the nuclear coordinates is zero. That is, the lowest energy point is obtained from the first order derivatives of energy with respect to the nuclear coordinates [56] that satisfy the condition

$$\frac{\partial E}{\partial R} = 0. \tag{3.1}$$

In the ground state geometries, the energy gaps E_{gap} are estimated from the difference between the highest occupied (HOMO) and lowest unoccupied (LUMO) molecular orbital eigen-energies ($\Delta\varepsilon_{H-L}$) in both gas phase and in solvents; these energy gaps can be compared to the chemical energy gaps as obtained with the use of cyclic voltammetry [73]. The convergence criteria of the self-consistent field method (SCF) used by Gaussain is that the maximum component of the force must be below the cutoff value of 0.00045 N, the root-mean-square of the force must be below 0.0003 N, the calculated displacement for the next step must be smaller than the cutoff value of 0.0018 N, and the root-mean-square of the displacement for the next step must be below the cutoff value of 0.0012 N [56].

To study the solvent effect, we used the keyword SCRF = (PCM, solvent) which applies the self-consistence reaction field method with using the Polarizable Continuum Model (PCM), which performs the Integral Equation Formalism (IEF-PCM) calculations [53]. The solvent for the PCM calculations can be specified using the normal solvent options, the solvent name keyword or dielectric constant of the solvent by using EPS=e keyword; we have used the name of the solvent in our calculations. The solvents considered are chloroform and methanol in both F and C calculations. In addition to chloroform and methanol, chlorobenzene and o-dichlorobenzene were used in the calculations of PTB7 and PBnDT-DTBT monomers.

The total electronic (ground state) dipole moments are also reported which give information about the charge polarizations in the polymer. They are calculated from the sum of the products of the charge and the distance between the two charges,

$$\mu = \sum_{i=1}^{n} Q_i R_i; \tag{3.2}$$

it is expected that the dipole moment will increase with increasing the solvent polarity (increasing the dielectric constant ϵ).

The TD-DFT method was used to compute the transition data for all the studied systems in both the gas phase and solvents; the keyword NStates=6 was used to calculate the first six excitation energies. The wavelengths and oscillator strengthes were obtained from the output files. The wavelengths and the lowest (singlet) excited state energies were compared with the corresponding optical (absorbtion) peak wavelengths and excitation energies (often referred as optical band gaps) when possible.

Both the input and output geometries of the systems have been obtained with using GaussView 3.0 software [74]. This software is used to visualize the geometries, measure the bond lengths, and the dihedral angles of the systems in the gas phase and in solvents. The bond lengths measures the charge delocalization along the back bone. The dihedral angles tell us how planar the polymers are.

B3LYP exchange-correlation functional with charge (= +1) and opt keyword were used to get the cation geometry, which is later used to calculate the hole reorganization energy (as discussed in Chapter 2) of PTB7 and PBnDT-DTBT monomers in the gas phase and in above mentioned solvents. All the calculations are dealing with closed-shell (neutral) polymer systems except the calculations of the reorganization energy which are dealing with the opened-shell (cation) systems in addition to closed-shell systems.

Chapter 4

Fluorene and Carbazole Oligomers

In this chapter we apply DFT method to obtain the ground state electronic structure of fluorene (F) and carbazole (C) oligomers (consisting of 1-4 monomers) in the gas phase and in solvents. For solvent effect we use PCM model (as discussed in Chapter 2) with chloroform (ϵ=4.71) and methanol (ϵ=32.61) [71] as solvents. TD-DFT is used to investigate the excited state properties of the oligomers in the gas phase and solvents. Since electronic properties are closely related to geometries of the systems, we discuss the geometrical parameters such as bond lengths and dihedral angles in both the gas phase and in the mentioned solvents.

4.1 Fluorene Oligomers

Fluorene oligomers belong to a chemical group called polycyclic aromatic hydrocarbons. A fluorene monomer contains 13 carbon atoms (two phenyl rings and carbon atom connecting them) along the chain backbone and two side groups (alkyl chains of various lengths, typically octyl chains are used) as is shown in Fig. 4.1. Polyfluorenes (PF) have been shown to be promising candidates for all-color light-emitting

diodes [73, 75] due to their efficient blue-to-green light emission, good solubility in most organic solvents, and good thermal stability.

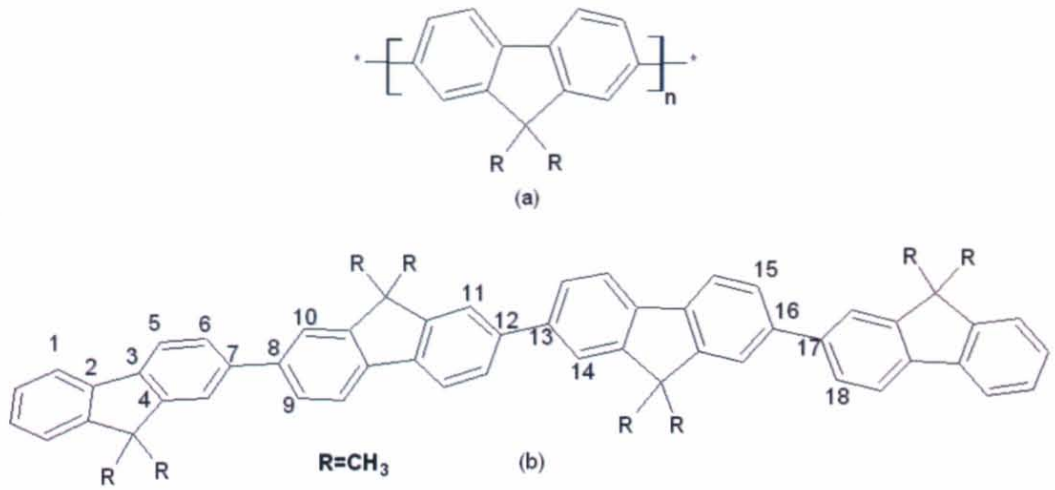

Figure 4.1: The chemical structures of (a) monomer and (b) four monomers of fluorene. 1, 2, 3, ... label the carbon atoms of fluorene oligomer, that are used in definitions of the dihedral angles and inter-ring distances.

In the DFT ground state computations, in the initial structure, all bonds are set to be equal along the backbone. The geometry optimization, which minimizes the energy, modifies the molecular bonds in such a way that the output structure has alternating shorter and longer bonds along the backbone. In all calculations, we substitute 9,9′-dioctyl side groups with 9,9′-dimethyl side groups to reduce the computation time. It has been shown that the length of alkyl chains does not significantly affect the equilibrium geometries and electronic properties of F polymers in vacuum [76]. The attachment of the side group to the conjugated backbone enhances the solubility of the polymer [26].

4.1.1 Ground State Structure of Fluorene Oligomers

The chemical structure and labeling atoms of fluorene oligomer are depicted in Figure 4.1. The B3LYP/6-31G^* optimized ground state HOMO (ε_{HOMO}) and LUMO (ε_{LUMO}) energies (in eV) in the gas phase and in the solvent are listed in Table 4.1. In the gas phase, the HOMO eigenvalues are increasing and LUMO eigenvalues are decreasing as the chain length gets longer. The HOMO-LUMO gaps $\Delta\varepsilon_{(H-L)}$ decrease as the oligomers get longer. The HOMO and LUMO eigenvalues and their differences display linear behavior as function of the inverse chain length (1/n, where n is the number of monomers in a given oligomer). By extrapolating them to infinity (i.e. as n$\rightarrow \infty$), their corresponding polymer values can be obtained from the intercept since 1/n$\rightarrow$ 0 as n$\rightarrow \infty$. We obtain the values of -4.9 eV for the HOMO and -1.7 eV for the LUMO energies, which are higher than the reported experimental data for fluorene polymer (film) ($\varepsilon_{HOMO} = -5.7$ eV, $\varepsilon_{LUMO} = -2.50$ eV [77]). For illustration purposes the HOMO-LUMO energy differences are plotted as a function of the inverse chain length in Fig. 4.2. The extrapolation to infinite chain length gives a value of 3.2 eV for the fluorene polymer band gap value in the gas phase which is in good agreement with the reported experimental (mostly obtained with the use of cyclic voltammetry) values of 3.2-3.5 eV [78]. Others calculated similar values for the HOMO-LUMO differences [79].

As can be seen from Table 4.1, in the solvent, chloroform lowers the HOMO and LUMO energies by about 0.1 to 0.14 eV in comparison to the gas phase values and methanol decreases the HOMO and LUMO energies (from 0.05 to 0.1 eV) more than chloroform. The solvent affected HOMO-LUMO gaps are also plotted in Fig. 4.2 as a function of reciprocal chain length. At n=3 and n=4 the solvent effect on the gaps is a bit more noticeable than at n=1 and n=2, but in contrast to the HOMO and

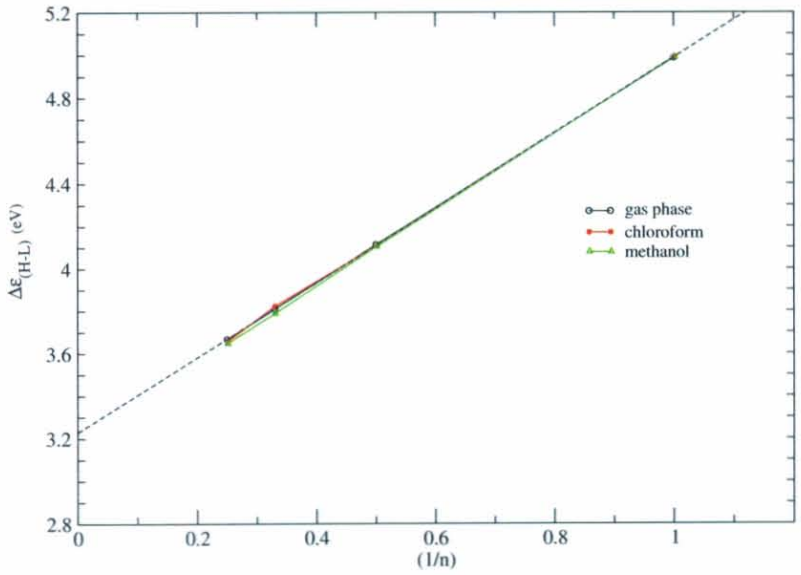

Figure 4.2: The HOMO-LUMO gaps $\Delta\varepsilon_{H-L}$ as function of the inverse chain length n of F oligomer in the gas phase, in chloroform solution, and in methanol solution.

Table 4.1: The negative of the HOMO ($-\varepsilon_{HOMO}$) and LUMO ($-\varepsilon_{LUMO}$) energies and their differences ($\Delta\varepsilon_{(H-L)}$) (in eV) for fluorene oligomers in gas phase and in a solvent as obtained using B3LYP/6-31G^* method.

$(F)_n$	gas phase /solvent	$-\varepsilon_{HOMO}$	$-\varepsilon_{LUMO}$	$\Delta\varepsilon_{(H-L)}$
	gas phase	5.731	0.743	4.988
n = 1	chloroform	5.825	0.834	4.991
	methanol	5.876	0.884	4.992
	gas phase	5.326	1.213	4.113
n = 2	chloroform	5.420	1.312	4.108
	methanol	5.474	1.369	4.105
	gas phase	5.188	1.379	3.809
n = 3	chloroform	5.242	1.419	3.823
	methanol	5.332	1.542	3.790
	gas phase	5.126	1.459	3.667
n = 4	chloroform	5.214	1.558	3.656
	methanol	5.268	1.619	3.649

LUMO energies, the HOMO-LUMO energy differences remain virtually unaffected by the presence of a solvent.

Table 4.2 lists the labeled dihedral angles (Φ in degrees) and the inter-ring distances (r in Å) (see Fig. 4.1b) for the F oligomer containing four monomers (F_4). F oligomers form twisted (nonplanar) structures in their ground states mostly due to rotations about the inter-ring bonds ($r(7,8)$, $r(12,13)$ etc. in Fig. 4.1b) between monomers. The dihedral angle between the two phenyl rings in a F monomer is fixed by ring-bridged atoms and is nearly zero (no more than 1° [73]). Table 4.2 shows that all the listed dihedral angles in the gas phase are close to 143°. Chloroform and methanol increase the dihedral angles by approximately 1° to become 144°.

The inter-ring distances are not changed by the solvent effect, they remain close to 1.48 Å in both gas phase and in the solvents (chloroform and methanol).

The magnitudes of an electronic dipole moment are also listed in the Table 4.3 for the various F oligomers. They are plotted as a function of n in Fig. 4.3. This figure shows that the magnitude of the dipole moments does not decrease or increase smoothly with chain length as was observed in the case of energies and wavelengths. Instead, a sawtooth pattern is observed. This pattern correlates with even- and odd-monomer oligomers. That is, odd-monomer F oligomers (with n=1 and 3) have larger dipole moments which are increasing with n, whereas even-monomer F oligomers (with n=2 and 4) have smaller dipole moments that are decreasing with n. This is clearly due to the fact that according to Eq. (3.2), in the odd-monomer oligomers the products of charge and distance are not canceling each other as well as in even-monomer oligomers (since the even numbered oligomers are more symmetric than the odd numbered oligomers). In this case the magnitude of a dipole moment for the polymer (corresponding to a very long oligomer) will depend on whether the number of monomers is odd or even. One general trend is that, for a given F oligomer, the electronic dipole moment is increasing with increased solvent polarity, i.e. when ϵ is large as in the methanol solution (ϵ=32.61) the dipole moment is also large compared to the one in the chloroform solution (ϵ=4.71) or in the gas phase.

4.1.2 Excited State Properties of Fluorene Oligomers

The TD-DFT/B3LYP/6-31G^* method has been used to obtain the energies of the first six singlet excited states of F oligomers (n=1-4) in the gas phase, and in chloroform and methanol solutions. Only the data for the first lowest singlet excited state is given in the Table 4.4. The calculations of excitation energies are performed at the

Table 4.2: The dihedral angles Φ (in deg) and inter-ring distances r (in Å) for F_4 as obtained using B3LYP/6-31G^* method. For labeling of angles and bonds see Fig. 4.1b.

gas phase /solvent	$\Phi(6,7,8,9)$ $r(7,8)$	$\Phi(11,12,13,14)$ $r(12,13)$	$\Phi(15,16,17,18)$ $r(16,17)$
gas phase	142.97	-142.70	-142.16
	1.483	1.483	1.483
chloroform	143.87	-143.48	-143.07
	1.484	1.484	1.484
methanol	144.51	-144.02	-143.58
	1.484	1.484	1.484

Table 4.3: The electronic dipole moment μ (in Debye) of fluorene oligomers as obtained using B3LYP/6-31G^* method.

(F_n)	gas phase /solvents	μ (Debye)
n = 1	gas phase	0.4265
	chloroform	0.4894
	methanol	0.5430
n = 2	gas phase	0.2852
	chloroform	0.3206
	methanol	0.3453
n = 3	gas phase	0.6152
	chloroform	0.6971
	methanol	0.7629
n = 4	gas phase	0.2020
	chloroform	0.2249
	methanol	0.2889

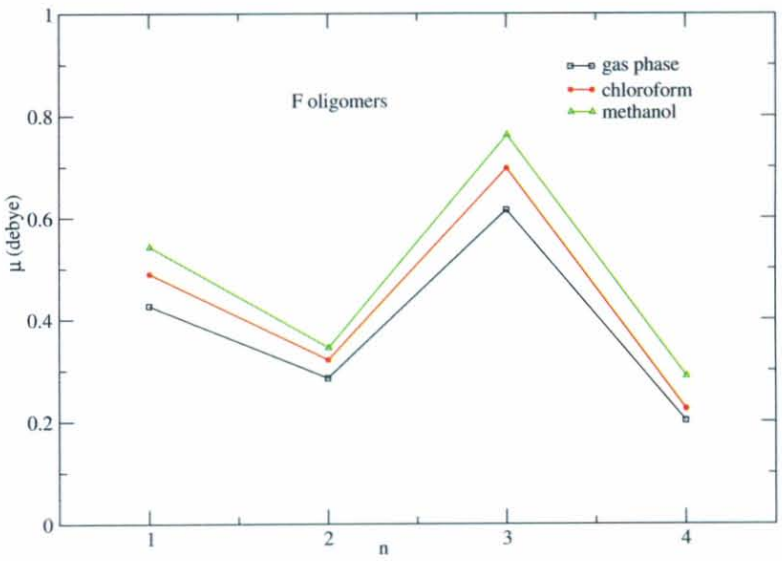

Figure 4.3: The electronic dipole moment μ of F oligomers versus n (the number of monomers) in the gas phase and in the solvents.

ground state equilibrium geometries. The lowest excitation energies (E_1 in eV), the absorption wavelengths (λ in nm), the oscillator strengths (f), and the characters of molecular orbitals (MO/character) involved in the lowest excitation of F oligomers are listed in the Table 4.4.

All electronic transitions ($S_0 \rightarrow S_1$) are of the $\pi - \pi^*$ type, that is, the excitation to the S_1 state exclusively corresponds to the electron promotion from the HOMO to the LUMO. The lowest excitation energies E_1 are also plotted as a function of chain inverse length in Fig. 4.4 in the gas phase and in solvents. In the gas phase, the slope is measured to be approximately 1.8 eV/(1/n) and the intercept is estimated to be 2.8 eV which is approximately 0.3 eV or more lower than the experimentally determined optical band gap (3.13-3.3 eV [73]). It should be noted that other methods such as the seminempirical ZINDO/S [81, 82] calculations obtained a value of 32755 cm^{-1} ($\simeq$4.0611 eV) for E_1 for a F dimer in the gas phase which again differs by 0.3 eV from our value. The presence of a solvent in general decreases the value of E_1. Chloroform decreases E_1 more than methanol by about 0.03 eV in most cases. This effect of the solvents on E_1 is shown in Fig. 4.4. In addition, from our calculations in Table 4.4, we notice that the calculated absorption wavelengths λ's in the gas phase and in the solvents increase with longer chain lengths (which agrees with E_1's decreasing with chain lengths since $E_1 \propto 1/\lambda$). The decrease in the wavelengths is very similar for both solvents, i.e., in the methanol solution F oligomers have absorption λ's ranging from 270 to 384 nm and in the chloroform solution the corresponding range is from 271 to 385 nm which again is not that different from the gas phase values (from 268 to 381 nm).

The excitation energies of the next five states have relatively small oscillator strength values (and hence most likely very low observable intensities); the $S_0 \rightarrow S_1$ transitions have the largest f's. Moreover, the oscillator strengths which are related

to the coupling of the lowest charge transferred $\pi - \pi^*$ singlet excited states to the ground states increase by about 1 with each addition of another monomer in both the gas phase and the solvents (see Table 4.4). Comparing to the gas phase and methanol values, chloroform has the largest f value and the lowest excitation energy for any given oligomer. This indicates that the absorption spectrum for F oligomers in chloroform (solvent with small dielectric constant) would have the highest intensity and lowest first excited state energies (and highest absorption wavelengths), but not by very much.

Table 4.4: The lowest singlet-singlet transition energies E_1 (in eV), the absorption wavelengths λ (in nm), the oscillator strengths f, and the molecular orbital character as obtained by using TD-B3LYP/6-31G^* method for fluorene oligomers in the gas phase and in solvents.

(F_n)	gas phase /solvent	transition	E_1 (eV)	λ (nm)	f	MO/character
	gas phase	$S_0 \rightarrow S_1$	4.6207	268.32	0.2699	$HOMO \rightarrow LUMO$
n = 1	chloroform	$S_0 \rightarrow S_1$	4.5629	271.72	0.4414	$HOMO \rightarrow LUMO$
	methanol	$S_0 \rightarrow S_1$	4.5828	270.54	0.4040	$HOMO \rightarrow LUMO$
	gas phase	$S_0 \rightarrow S_1$	3.7463	330.95	1.2739	$HOMO \rightarrow LUMO$
n = 2	chloroform	$S_0 \rightarrow S_1$	3.6699	337.84	1.5063	$HOMO \rightarrow LUMO$
	methanol	$S_0 \rightarrow S_1$	3.6900	336.00	1.4607	$HOMO \rightarrow LUMO$
	gas phase	$S_0 \rightarrow S_1$	3.4115	363.43	2.0704	$HOMO \rightarrow LUMO$
n = 3	chloroform	$S_0 \rightarrow S_1$	3.3537	369.69	2.3190	$HOMO \rightarrow LUMO$
	methanol	$S_0 \rightarrow S_1$	3.3695	367.96	2.2740	$HOMO \rightarrow LUMO$
	gas phase	$S_0 \rightarrow S_1$	3.2559	380.80	2.8263	$HOMO \rightarrow LUMO$
n = 4	chloroform	$S_0 \rightarrow S_1$	3.2129	385.89	3.0718	$HOMO \rightarrow LUMO$
	methanol	$S_0 \rightarrow S_1$	3.2252	384.43	3.0284	$HOMO \rightarrow LUMO$

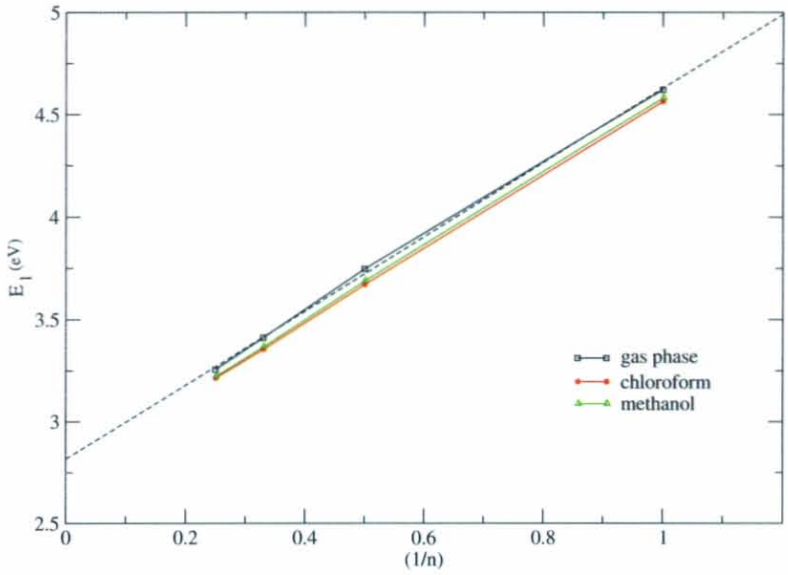

Figure 4.4: The lowest excitation energies of F in the gas phase, in chloroform solution, and in methanol solution versus the inverse chain length 1/n.

4.2 Carbazole Oligomers

Carbazole has a tricyclic chemical structure, 2 phenyl rings fused on either side of a five-membered nitrogen-containing ring (as shown in Fig. 4.5). C polymer and its derivatives have elicited considerable attention by scientists for the past 30 years. This is mainly due to the finding that C oligomers and polymers play the role of chromophores in polymeric systems such as poly(N-vinylcarbazole) which is one of the most sensitive photoconductive organic polymers [83, 84]. Others such as poly(2,7-carbazole) and its derivatives have many applications in solar cells [85, 86]. Similarly to F oligomers, we replace, in all computations, the long alkyl chain which is typically bonded to the nitrogen atom of C oligomer with a methyl (CH_3) side group.

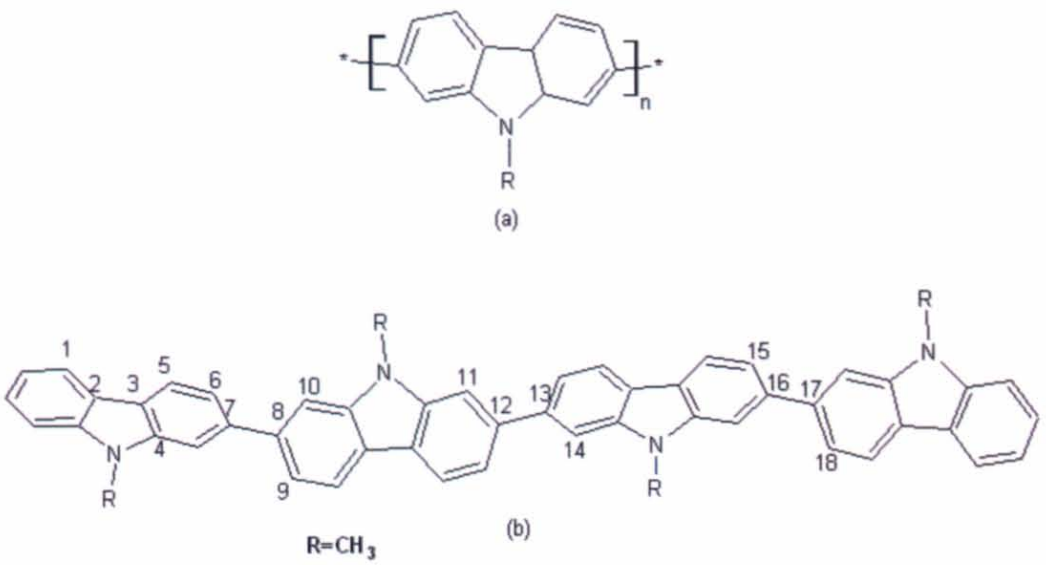

Figure 4.5: The chemical structures of (a) carbazole monomer, and (b) four monomers of carbazole. 1, 2, 3, ... label carbon atoms of carbazole oligomer, that are used in definitions of the dihedral angles and inter-ring distances.

4.2.1 Ground State Structure of Carbazole Oligomers

The optimized B3LYP/6-31G^* ground state HOMO (ε_{HOMO}) and LUMO (ε_{LUMO}) energies (in eV) in the gas phase and in the solvent of C oligomers are listed in Table 4.5. As for F oligomers, the HOMO and LUMO energies are lowered by the presence of a solvent. Methanol decreases the HOMO and LUMO eigenvalues the most (they become more negative), followed by chloroform and the gas phase. The calculated HOMO and LUMO energy levels are identical to another theoretical study that used the same method in the gas phase [87]. Again, as for F oligomers, the HOMO-LUMO

band gaps $\Delta\varepsilon_{H-L}$ of C oligomers are plotted as a function of the reciprocal chain length 1/n in Fig. 4.6. From the data reported in the Table 4.5, we see that the HOMO-LUMO band gaps are slightly lowered in solutions. This effect is shown in Fig. 4.6. The extrapolated band gap for the C polymer in the gas phase is estimated to be 3.3 eV which is 0.2 eV larger than the reported band gap (3.1 eV) as obtained electrochemically in cyclic voltammetry experiments [88]. It should be noted that the estimated band gap of the carbazole polymer is much larger than the suggested band gap for the ideal polymer for the photovoltaic applications which is reported as 1.5 eV [89, 90] (see Chapter 1). For this reason, nowdays, carbazole derivatives (co-polymers) are used in solar cells.

The labeling of the C oligomer structure is illustrated in the Fig. 4.5b. The dihedral angles (Φ in degrees) and the bond lengths (r in Å) of C_4 are listed in Table 4.6. The C oligomers have a nonplanar structure in their ground states [91]. A slightly more planar conformation of C oligomers is observed in methanol and chloroform solutions in comparison to the conformation of C oligomers in the gas phase (144° or 143° versus 142° respectively). The bond lengths are not effected by the solvent.

Table 4.7 lists the electronic dipole moments μ (in Debye) of carbazole oligomers. Chloroform and methanol increase the electronic dipole moments of carbazole oligomers compared to the gas phase values. In Fig. 4.7 the magnitudes of electric dipole moment are plotted as a function of n for C oligomers. As above, a sawtooth pattern is observed. The pattern can again be explained by noting that even-monomer oligomers are more symmetric than odd-monomer oligomers and hence even-monomer oligomers have lower dipole moments than the odd-monomer oligomers. Typically solvents increase the dipole moments. Methanol gives the biggest rise to μ which is larger in comparison to the gas phase values by about 0.8 Debye for the trimer and 0.6, 0.4,

Table 4.5: The negative of the HOMO $-\varepsilon_{HOMO}$ and LUMO $-\varepsilon_{LUMO}$ energies and their differences $\Delta\varepsilon_{(H-L)}$ (in eV) for carbazole oligomers using the B3LYP/31-6G^* method.

(C_n)	gas phase /solvent	$-\varepsilon_{HOMO}$	$-\varepsilon_{LUMO}$	$\Delta\varepsilon_{(H-L)}$
n = 1	gas phase	5.319	0.624	4.692
	chloroform	5.410	0.747	4.663
	methanol	5.457	0.805	4.652
n = 2	gas phase	5.243	1.040	4.203
	chloroform	5.369	1.174	4.195
	methanol	5.433	1.244	4.189
n = 3	gas phase	5.097	1.200	3.897
	chloroform	5.228	1.336	3.892
	methanol	5.293	1.412	3.881
n = 4	gas phase	5.029	1.273	3.752
	chloroform	5.158	1.412	3.746
	methanol	5.224	1.487	3.737

Table 4.6: The dihedral angles Φ (in deg) and the inter-ring distances r (in Å) for C_4 obtained using the B3LYP/6-31G^* method. For labeling of angles and bonds see Figure 4.5b.

gas phase /solvent	$\Phi(6,7,8,9)$ $r(7,8)$	$\Phi(11,12,13,14)$ $r(12,13)$	$\Phi(15,16,17,18)$ $r(16,17)$
gas phase	-141.756	-141.959	141.772
	1.485	1.485	1.485
chloroform	-142.923	-142.970	143.010
	1.486	1.486	1.486
methanol	-143.715	-143.792	143.601
	1.486	1.486	1.486

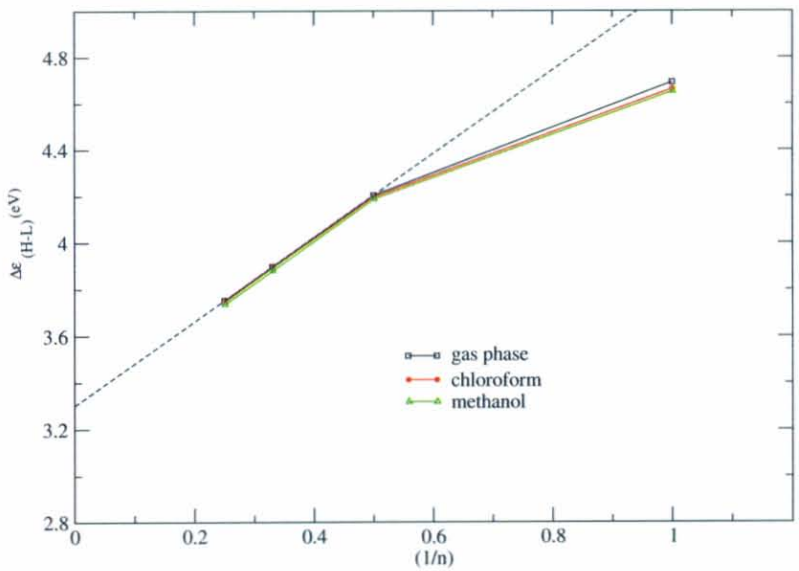

Figure 4.6: The HOMO-LUMO gaps of C oligomer versus 1/n in the gas phase and in solvents.

Table 4.7: The electronic dipole moment (in Debye) of carbazole oligomers as obtained using the B3LYP/6-31G^* method.

(C_n)	gas phase /solvents	μ (Debye)
	gas phase	1.8323
$n = 1$	chloroform	2.1596
	methanol	2.4640
	gas phase	1.1837
$n = 2$	chloroform	1.3626
	methanol	1.5623
	gas phase	2.4711
$n = 3$	chloroform	2.8793
	methanol	3.2990
	gas phase	0.7417
$n = 4$	chloroform	0.9114
	methanol	0.9837

0.2 Debye for the monomer, dimer, and tetramer respectively. Chloroform increases the dipole moments by approximately half of these increments as can be seen in Fig. 4.7.

4.2.2 Excited State Properties of Carbazole Oligomers

The TD-DFT method has been employed on the fully geometry optimized ground state structures of C oligomers (n=1-4) to obtain the energies of the first 6 singlet-singlet electronic transitions. The properties of the lowest $S_0 \rightarrow S_1$ transitions of C oligomer in the gas phase and in solvents (chloroform and methanol) are summarized in Table 4.8. The $S_0 \rightarrow S_1$ transitions are HOMO→LUMO type except for the dimer (n=2) where lowest transitions involve HOMO-1→LUMO. These HOMO-1→LUMO

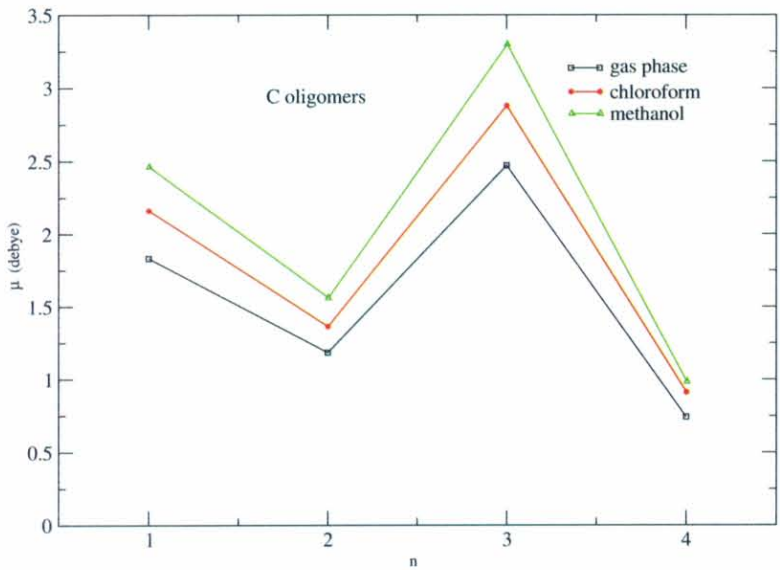

Figure 4.7: The electric dipole moment μ of C oligomers versus n in the gas phase, chloroform, and methanol solutions.

transitions are almost forbidden due to their very small oscillator strength f values and hence they will have low intensity in optical spectra. The $S_0 \rightarrow S_2$ transitions of the dimer have somewhat higher oscillator strength (they are of HOMO-2→ LUMO type) but again they will also not be readily observed in the optical spectral due to their low intensity (because of the low value of f). The HOMO→ LUMO type of transitions ($S_0 \rightarrow S_3$) of the dimer have the highest intensity as suggested by f values and expected to be the most readily observed. The carbazole monomer (n=1) has also very low HOMO→LUMO intensity (very small f value). The HOMO→ LUMO transitions of a C trimer and tetramer are expected to have high intensity (see Table 4.8).

Table 4.8: The lowest singlet-singlet transition energies E_1 in (eV), the absorption wavelengths λ (in nm), the oscillator strengths f, and molecular orbital characters for the carbazole oligomer using the TD-B3LYP/31-6G^* method.

(C_n)	gas phase /solvent	transition	E_1[(a)] (eV)	λ (nm)	f	MO/Character
	gas phase	$S_0 \rightarrow S_1$	4.0463	306.42	0.0315	$HOMO \rightarrow LUMO$
n = 1	chloroform	$S_0 \rightarrow S_1$	4.0111	309.10	0.0458	$HOMO \rightarrow LUMO$
	methanol	$S_0 \rightarrow S_1$	3.9965	310.23	0.0424	$HOMO \rightarrow LUMO$
	gas phase	$S_0 \rightarrow S_1$	3.7582	329.91	0.0054	$HOMO-1 \rightarrow LUMO$
	chloroform	$S_0 \rightarrow S_1$	3.7215	333.15	0.0100	$HOMO-1 \rightarrow LUMO$
	methanol	$S_0 \rightarrow S_1$	3.7072	334.44	0.0071	$HOMO-1 \rightarrow LUMO$
	gas phase	$S_0 \rightarrow S_2$	3.7656	329.26	0.1238	$HOMO-2 \rightarrow LUMO$
n = 2	chloroform	$S_0 \rightarrow S_2$	3.7219	333.12	0.3816	$HOMO-2 \rightarrow LUMO$
	methanol	$S_0 \rightarrow S_2$	3.7103	334.16	0.1934	$HOMO-2 \rightarrow LUMO$
	gas phase	$S_0 \rightarrow S_3$	3.8258	324.07	1.0039	$HOMO \rightarrow LUMO$
	chloroform	$S_0 \rightarrow S_3$	3.7660	329.22	1.0578	$HOMO \rightarrow LUMO$
	methanol	$S_0 \rightarrow S_3$	3.7834	327.71	1.1647	$HOMO \rightarrow LUMO$
	gas phase	$S_0 \rightarrow S_1$	3.4970	354.54	1.9536	$HOMO \rightarrow LUMO$
n = 3	chloroform	$S_0 \rightarrow S_1$	3.4439	360.01	2.2734	$HOMO \rightarrow LUMO$
	methanol	$S_0 \rightarrow S_1$	3.4615	358.18	2.1908	$HOMO \rightarrow LUMO$
	gas phase	$S_0 \rightarrow S_1$	3.3456	370.59	2.7649	$HOMO \rightarrow LUMO$
n = 4	chloroform	$S_0 \rightarrow S_1$	3.3069	374.93	3.0755	$HOMO \rightarrow LUMO$
	methanol	$S_0 \rightarrow S_1$	3.3217	373.25	3.0130	$HOMO \rightarrow LUMO$

As for F oligomers, excitation energies corresponding to HOMO→LUMO transitions decrease with longer oligomer chains in the gas phase and in the considered solvents. The energies of HOMO→LUMO transitions are plotted as a function of 1/n

[(a)]For a dimer (n=2) we also include E_2 and E_3, see text for discussion.

in the Figure 4.8. As is shown in the figure, these excitation energies are somewhat affected by presence of the solvent. For n=1 methanol lowers E_1 more than chloroform. This trend is inverted for n larger than 1, i.e. in the C dimer, trimer, and tetramer chloroform lowers the excitation energy corresponding to the HOMO→LUMO transition more than methanol (see Table 4.8). The extrapolated value of the energies corresponding to HOMO→LUMO transitions gives the so called optical band gap for the polymer (PC) which in this case is close to 3 eV (2.9 eV) which should be compared to the experimental value of 3.3 eV [88].

The absorption wavelength λ for a given C oligomer is red-shifted by presence of the solvent in comparison to the gas phase values (see Table 4.8). The calculated λ of the C dimer in the gas phase has the value of 330 nm which is comparable to the value 332 nm of $S_0 \rightarrow S_1$ transition of the dimer calculated by Belletête and coworkers [92] using the ZINDO/S semi-empirical method performed on the HF/ 6-31G^* optimized geometry. The calculated λ of the dimer in the gas phase is consistent with the reported experimental values (345, 360 nm) [93].

4.3 Conclusions

DFT and TD-DFT methods were used to perform the calculations of F and C oligomers in the gas phase. The SCRF method (PCM model) was employed to study the solvent effect on the electronic properties of F and C oligomers. The calculations for both oligomers show that the HOMO's are increasing (more positive) and LUMO's are decreasing (more negative) with increasing chain length in the gas phase and in the considered solvents. The HOMO-LUMO gaps are decreased in most cases when chloroform and methanol are present. All the transitions of $S_0 \rightarrow S_1$ correspond to the promotion of electron from HOMO to LUMO and they are of $\pi - \pi^*$ type in both

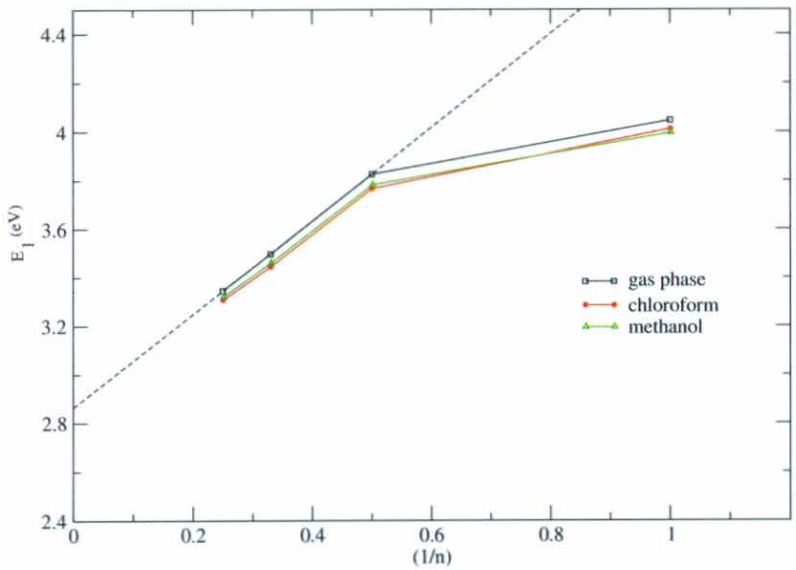

Figure 4.8: The lowest excitation energies E_1 which correspond to HOMO→LUMO transitions of C oligomers versus the reciprocal chain length 1/n in the gas phase, and in chloroform solution and in methanol solution.

the gas phase, and when solvents are present. Except for the C dimer, the $S_0 \rightarrow S_1$ transitions are from HOMO-1 to LUMO (and are forbidden according to the small values of f's). The lowest excitation energies are decreased by the presence of solvents relative to the gas phase values. $S_0 \rightarrow S_1$ transitions are red-shifted by the presence of solvents. Consequently, the presence of a solvent enhances the opportunity of getting low-band gap polymers required to design more efficient and cheaper devices.

Chapter 5

PTB7 Polymer

In this chapter we use the same methods as those used in Chapter 4 to investigate the solvent effect on the electronic structure of the monomer of poly[[4,8-bis[(2-ethylhexyl) oxy]benzo[1,2-b:4,5-b']dithiophene-2,6-diyl][3-fluoro-2-[(2-ethyl-hexyl) carbonyl]thieno[3,4-b] thiophenediyl]] (PTB7). In addition, we use the B3LYP/6-31G^* neutral and radical cation geometries of PTB7 to calculate the reorganization energy for hole transport λ_h (as discussed in Chapter 2) and see how this energy is affected by the presence of solvents in the calculations. The considered solvents are chloroform, chlorobenzene, o-dichlorobenzene, and methanol (the corresponding dielectric constant values are 4.71, 5.69, 9.99 and 32.61 respectively [71]).

5.1 The PTB7 Polymer

PTB7 is a semiconducting polymer based on alternating ester substituted thieno[3,4-b]thiophene and benzodithiophene units. The chemical structure and labeling atoms of PTB7 are shown in Fig. 5.1. In general, benzodithiophene polymers (PTBs) have been shown to be very promising polymers as candidates for bulk heterojunction poly-

mer/fullerides solar cells [94]. This type of solar cell is composed of electron-donating semiconducting polymer and electron-withdrawing fullerides as active layers [40]. The most recent study [40] shows that a PCE of 7.4% can be achieved using PTB7 (as a donor) with $PC_{71}BM$ (as an acceptor) in the presence of a solvent such as a mixture of chlorobenzene and 1,8-diiodooctane. This high PCE is due to the low band gap of PTB7 which is about 1.6 eV [40], providing efficient absorption around the region with the highest photon flux of the solar spectrum (about 700 nm). Moreover, the introduction of fluorine into the thien[3,4-b]thiophene (see the Fig. 5.1) provides the polymer with a low HOMO energy level, which offers a large open-circuit voltage (V_{oc}) [94]. The long 2-ethylhexyl side chains provide PTB7 with good solubility in organic solvents. All these properties of PTB7 make it a very good candidate for BHJ solar cells. In order to decrease the computational time we have substituted the 2-ethylhexyl side chains with 2-methyl side chains. This substitution does not affect the equilibrium geometry, long side chains enhance the solubility of conjugated polymers [32, 26].

5.1.1 Ground State Structure of the PTB7 Monomer

The HOMO and LUMO energy levels and their differences of the PTB7 monomer are obtained using the B3LYP/6-31G^* method. The calculated values of these energy levels are listed in the Table 5.1. Solvents increase the negativity of HOMO and LUMO energy levels of the PTB7 monomer from -5.23 and -2.10 eV in the gas phase to -5.35 and -2.18 eV respectively in the methanol solution. The degree of lowering of the HOMO and LUMO energy levels correlates with increasing solvent polarity, that is, the higher the solvent dielectric constant (from chloroform $\rightarrow$ chlorobenzene $\rightarrow$ o-dichlorobenzene to methanol) the lower the HOMO and LUMO energy levels

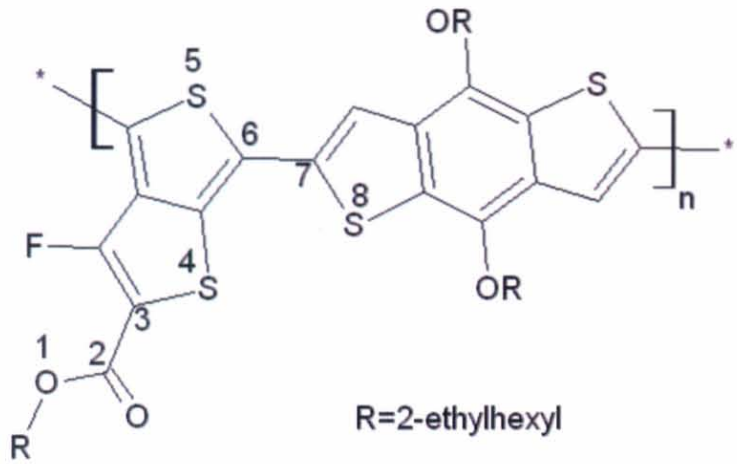

Figure 5.1: The chemical structure of the PTB7 monomer. 1, 2, 3, ... label different atoms of the PTB7 monomer, that are used in definitions of the dihedral angles and intra-molecular bonds.

of the PTB7 monomer. A comparison of the calculated HOMO energy of the PTB7

Table 5.1: The HOMO $-\varepsilon_{HOMO}$ and LUMO $-\varepsilon_{LUMO}$ energy levels and their difference $\Delta\varepsilon_{(H-L)}$ (in eV) for the PTB7 monomer using the B3LYP/6-31G^* method.

gas phase /solvent	$-\varepsilon_{HOMO}$	$-\varepsilon_{LUMO}$	$\Delta\varepsilon_{(H-L)}$
gas phase	5.226	2.097	3.129
chloroform	5.300	2.139	3.161
chlorobenzene	5.307	2.142	3.165
o-dichlorobenzene	5.326	2.170	3.156
methanol	5.346	2.181	3.165

monomer in the gas phase (−5.2 eV) with the experimental value of −5.1 eV as obtained with the use of cyclic voltammetry [40] shows good agreement. The LUMO energy level of the PTB7 monomer has a calculated value of −2.1 eV in the gas phase which is higher by more than 1 eV than its corresponding experimental value −3.3 eV [40]. In addition it should be noted that the calculated HOMO energy level of the PTB7 monomer in methanol solution is −5.35 eV, which probably is a good estimate of the actual value based on the above comparison and is in good agreement with the HOMO eigenvalue of an ideal donor polymer (−5.4 eV) in BHJ solar cells. The LUMO energy level of the PTB7 monomer in methanol solution is −2.18 eV, which is off by approximately 1.2 eV from the actual LUMO energy (should be closer to −3.4 eV for a real polymer) and is still considerably higher than the ideal value −3.9 eV [33] (see Chapter 1 for discussion of optimal (ideal) characteristics of solar cells). The HOMO-LUMO energy gap in solvents is approximately 3.16 eV, which is larger than the gas phase value 3.13 eV. The HOMO and LUMO energy levels of PTB7 monomer are plotted versus the dielectric constants ϵ's of the solvents in the Fig. 5.2.

The energy gaps versus the dielectric constants are plotted in Fig. 5.3.

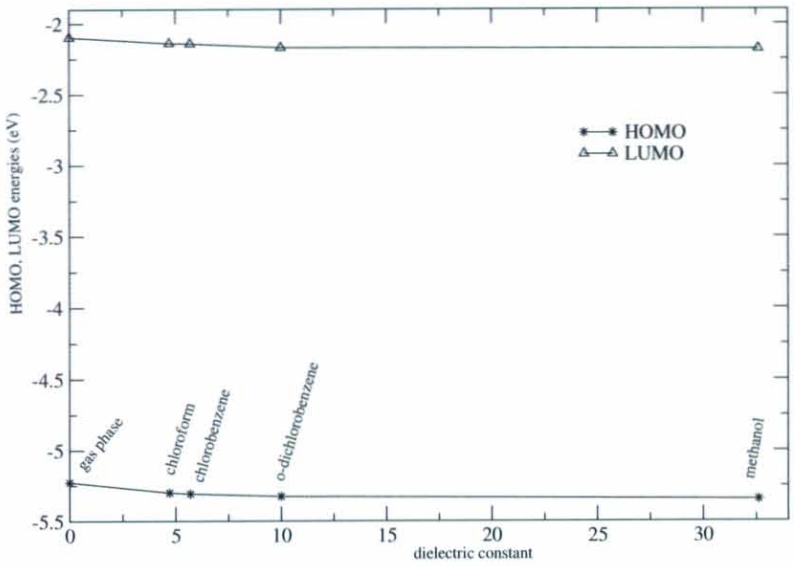

Figure 5.2: The HOMO and LUMO energy levels of the PTB7 monomer versus the dielectric constant of the solvents.

Next the ground state structure of the PTB7 monomer is discussed. Some of the dihedral angles of the PTB7 monomer for example $\Phi(1,2,3,4)$ and $\Phi(5,6,7,8)$, and intra-molecular bonds such as $r(2,3)$ and $r(6,7)$ can be seen in the Fig. 5.1 and their values are listed in the Table 5.2. The dihedral angle $\Phi(1,2,3,4)$ between the ester and thieno[3,4-b]thiophene units (see Fig. 5.1) remains around $-180°$ for all considered solvents (unchanged in comparison to the gas phase angle). The presence of chloroform, chlorobenzene and methanol solvents decreases the dihedral angle $\Phi(5,6,7,8)$ between thieno[3,4-b]thiophene and benzo[1,2-b:4,5-b']dithiophene units by more that $1°$ with reference to the gas phase angle of about $160°$, while the presence of solvent o-dichlorobenzene decreases the same angle by less than $1°$. The intra molecular bond

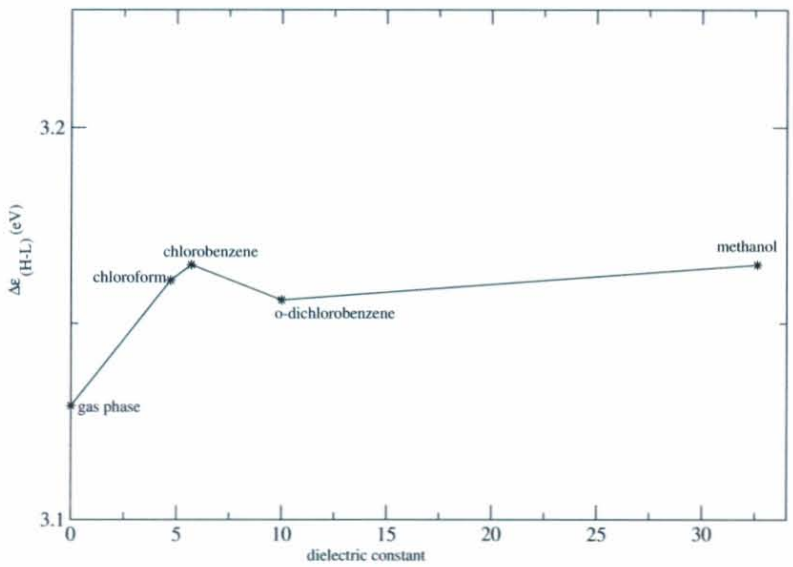

Figure 5.3: The HOMO-LUMO energy gap of the PTB7 monomer versus solvent's dielectric constant.

length $r(2,3)$ between the ester and thieno[3,4-b]thiophene is almost unaffected by the solvents and has the value of around 1.46 Å. The same trend is obtained for the bond length $r(6,7)$ between thieno[3,4-b]thiophene and benzo[1,2-b:4,5-b']dithiophene which is around 1.44 Åin the gas phase and in all considered solvents. It appears that the presence of the considered solvents does not have significant effect on the ground state (gas phase) geometrical structure of the PTB7 monomer.

In Table 5.2 the magnitudes of the dipole moment of the PTB7 monomer are included. As indicated in the Introduction, the polarity of the solvent is closely related to its dielectric constant. Hence, according to their dielectric constants, the order of the considered solvents in terms of their polarity from the highest to the lowest is as follows: methanol, o-dichlorobenzene, chlorobenzene, and chloroform. As expected the electronic dipole moment μ of the PTB7 monomer has the largest value in methanol solution since methanol has the highest polarity. This is followed by solutions of o-dichlorobenzene, chlorobenzene and chloroform, clearly indicating that the magnitude of dipole moment increases with the increased polarity of the solvent. In general, all the solvents give rise to a larger μ in comparison to the gas phase value by at least 1 Debye (see Table 5.2). The electronic dipole moment as a function of the dielectric constant of the solvents is plotted in the Fig. 5.4.

5.1.2 Excited State Properties of the PTB7 Monomer

The lowest singlet-singlet excited state properties of the PTB7 monomer are listed in Table 5.3, including the lowest excitation energy E_1, absorption wave-length λ, oscillator strength f, and MO character. All $S_0 \rightarrow S_1$ transitions in the gas phase and in the solvents are of $\pi \rightarrow \pi^*$ (HOMO$\rightarrow$ LUMO) type. These transitions have high intensities as suggested by their f values. The presence of chloroform, chloroben-

Table 5.2: The dihedral angles Φ (in deg), inter-ring distance r (in Å), and the electronic dipole moment μ (in Debye) for the PTB7 monomer as obtained using the B3LYP- 6-31G(d) method. For labeling angles and bonds see Fig. 5.1.

gas phase /solvent	$\Phi(1,2,3,4)$ r(2,3)	$\Phi(5,6,7,8)$ r(6,7)	μ (Debye)
gas phase	-179.79 1.469	160.09 1.445	3.4920
chloroform	-179.91 1.467	158.81 1.446	4.4718
chlorobenzene	-179.95 1.467	158.67 1.446	4.5324
o-dichlorobenzene	-179.98 1.468	159.11 1.446	4.6856
methanol	-179.99 1.467	158.80 1.446	4.9142

zene, and o-dichlorobenzene solvents decreases E_1 by 0.01 eV while the presence of methanol solvent increases E_1 by 0.01 eV as is shown in Fig. 5.5. As a result of

Table 5.3: The lowest transition energies E_1 (in eV), the absorption wavelengths λ (in nm), the oscillator strengths f, and molecular orbital MO character for the PTB7 monomer using the TD-B3LYP/6-31G^* method.

gas phase /solvent	transition	E_1 (eV)	λ (nm)	f	MO/Character
gas phase	$S_0 \rightarrow S_1$	2.8035	442.25	0.1958	$HOMO \rightarrow LUMO$
chloroform	$S_0 \rightarrow S_1$	2.7912	444.20	0.2821	$HOMO \rightarrow LUMO$
chlorobenzene	$S_0 \rightarrow S_1$	2.7897	444.44	0.2961	$HOMO \rightarrow LUMO$
o-dichlorobenzene	$S_0 \rightarrow S_1$	2.7884	444.64	0.2959	$HOMO \rightarrow LUMO$
methanol	$S_0 \rightarrow S_1$	2.8110	441.08	0.2564	$HOMO \rightarrow LUMO$

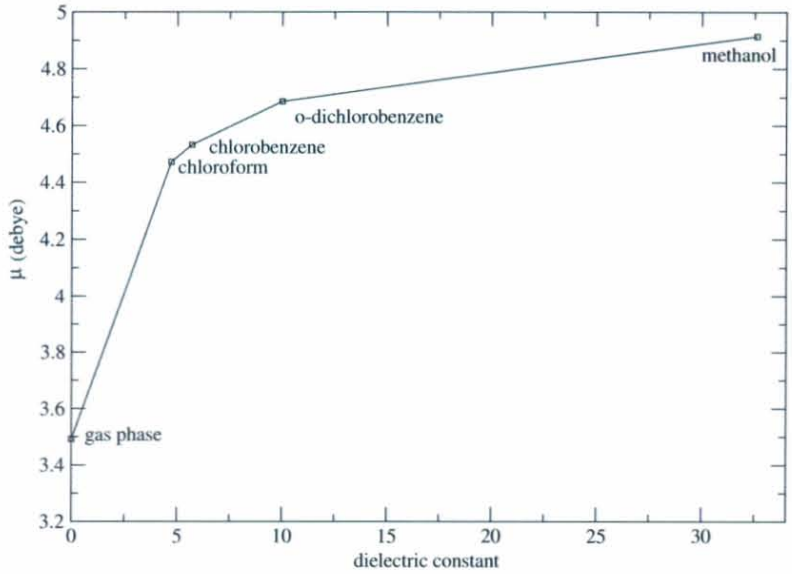

Figure 5.4: The dipole moment μ of the PTB7 monomer versus the solvent dielectric constant.

a different trend for chloroform, chlorobenzene and o-dichlorobenzene from the one observed for methanol in effecting E_1, the absorption wavelength λ is red-shifted in chloroform, chlorobenzene, and o-dichlorobenzene solutions and is blue-shifted in methanol solution in comparison to the gas phase wavelenght (see Table 5.3).

5.1.3 Hole Reorganization Energy λ_h of the PTB7 Monomer

The hole reorganization energy λ_h is an important parameter in hole transfer reactions and in understanding of hole mobility in a molecular crystal or polymer. PTB7 has a hole mobility of about 5.8×10^{-4} $cm^2V^{-1}s^{-1}$ [40]. In conjugated polymers, mobility is proportional to the charge hopping rate which, in turn (amongst other parameters), depends on the reorganization energy. The relation between the hole

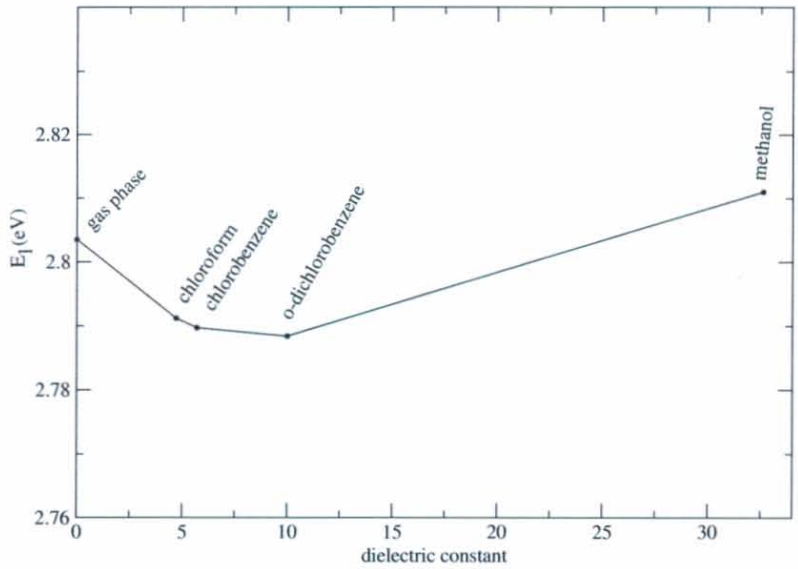

Figure 5.5: The lowest excitation energy E_1 of the PTB7 monomer versus the dielectric constant of the solvents.

transport rate and λ_h (Marcus-Hush theory), and how to calculate λ_h is discussed in Chapter 2. It should be noted that λ_h is also directly related to the binding energy of charge carriers such as polarons in conjugated polymers. That is, the polaron binding energy U_b is given by $U_b = \lambda_h/2$ for reactions where the acceptors and donors are of the same molecular types. Clearly a lower λ_h favors better solar cell performance since the binding energy of the polaron is also lowered and hence free charge transport is enhanced [95]. In this thesis, we investigate the solvent effect on the hole reorganization energy of PTB7 monomer. Table 5.4 lists λ_h (in meV) for PTB7 monomer in the gas phase and in the solvents. For completeness, the neutral and radical cation energy levels of PTB7 monomer which are used to calculate λ_h as discussed in Chapter 2 are shown in Fig. 5.6. The used solvents decreased λ_h of PTB7

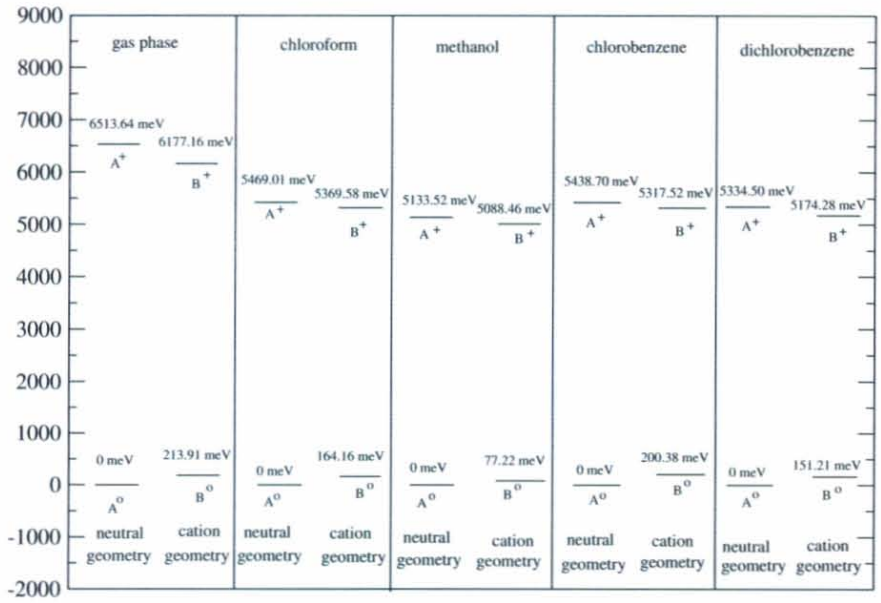

Figure 5.6: The energy levels of the ionic and the neutral PTB7 monomer in the gas phase and in the presence of solvents.

Table 5.4: The reorganization energy for hole transport of the PTB7 monomer in gas phase and in solvents as calculated using the B3LYP/6-31G^* method.

gas phase /solvent	λ_h (meV)
gas phase	550.39
chloroform	263.59
chlorobenzene	321.56
o-dichlorobenzene	311.43
methanol	122.28

monomer with respect to the gas phase value (550 meV). Methanol has the biggest effect on λ_h by lowering it by 428 meV relative to the gas phase value. Since smaller λ_h corresponds to higher transfer rate according to the Marcus-Huss theory (mainly due to lower polaron binding energy; see Chapter 2), then it can be concluded that methanol is the best solvent for the most efficient hole transport rate in solar cells made of PTB7 polymer and fullerenes. The effect of the solvents on λ_h is plotted in Fig. 5.7.

5.2 Conclusions

The energy levels (HOMO and LUMO) of PTB7 monomer become more negative in the presence of solvents. The energy gap is slightly bigger in the presence of all solvents than in the gas phase, but it does not depend on the type of a solvent (i.e. all solvents increase the energy gap by similar amounts). In all the solvents the ground state electronic dipole moment is increased and it is affected by solvent's polarity (a larger dipole moment is obtained with larger dielectric constant). The lowest singlet-singlet transition energies are lowered when solvents are used except

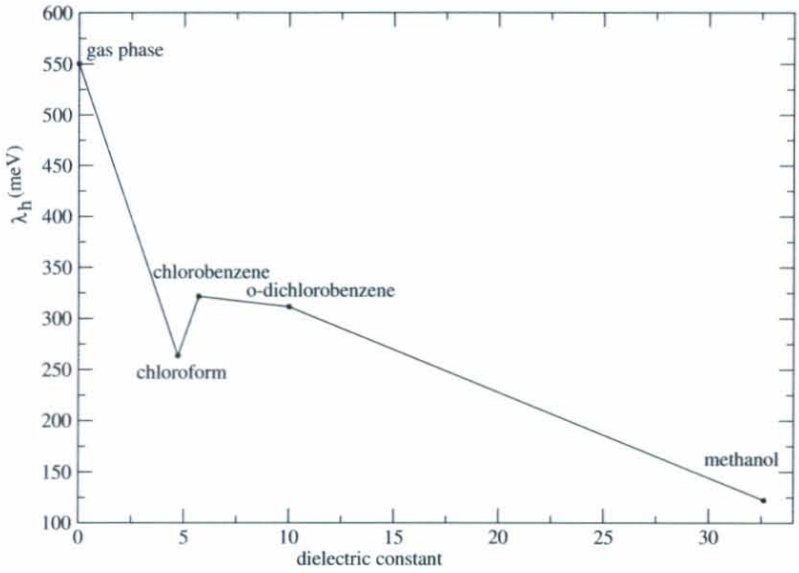

Figure 5.7: The reorganization energy for hole transport of the PTB7 monomer versus the dielectric constant of the considered solvents.

for methanol, i.e. the wavelength is red-shifted in chloroform, chlorobenzene, and o-dichlorobenzene, but in methanol, it is blue-shifted relative to the gas phase. The hole transport rate of PTB7 monomer is enhanced by using the solvent which lowers the hole reorganization energy. Methanol is the best for hole transport of PTB7 monomer. In the previously mentioned study [40], when the solvent chlorobenzene was used, a PCE of 3.92% was achieved. When o-dichlorobenzene was used, a PCE of 6.22% was obtained. This higher PCE in o-dichlorobenzene can be in part, justified by the effect of o-dichlorobenzene on λ_h of the PTB7 monomer, which lowers λ_h more than chlorobenzene (see Table 5.4). It is expected that the use of methanol as a solvent might increase the PCE even more.

Chapter 6

PBnDT-DTBT Polymer

Chapter 6 investigates the solvent effect on the electronic structure and some transport properties of the monomer of poly[4,8-dialkylbenzo[1,2-b:4,5-b']dithiophene-4,7-di(2-thienyl)-2,1,3-benzothiadiazole] (PBnDT-DTBT). As mentioned in Chapter 3 the PCM solvation model and B3LYP/6-31G^* method are used to perform the computations. The same solvents as in Chapter 5 are employed in this chapter: chloroform, chlorobenzene, o-dichlorobenzene, and methanol. Also as before we study the effect of the various solvents on the HOMO and LUMO energy levels, the corresponding (HOMO-LUMO) energy gap, ground state electronic dipole moment, lowest state excitation energy, and hole reorganization energy of the PBnDT-DTBT monomer.

6.1 PBnDT-DTBT Polymer

PBnDT-DTBT polymer consists of benzo[1,2-b:4,5-b']dithiophene units (BnDT) and 4,7-di(2-thienyl)-2,1,3-benzothiadiazole units (DTBT) (see Fig. 6.1 for its labeled chemical structure). Low-band gap conjugated polymers have attracted considerable interest in the recent years. One way to obtain low band gaps in conjugated poly-

mers is to create an alternating arrangement of aromatic and quinoid units along the polymer chain, thereby reducing the bond length alternation [96, 97, 98]. For example, electron-deficient quinoid heterocycles (e.g., benzothiadiazole, quinoxaline, oxazole, etc) have been alternated with aromatic electron-rich rings (e.g., phenylene, thiophene, and pyrrole) to prepare low band gap polymers. This type of (chemical) design has been implemented in PBnDT-DTBT which has an electrochemical band gap of 2.16 eV (with $\varepsilon_{HOMO} = -5.33$ and $\varepsilon_{LUMO} = -3.17$) and an approximate optical band gap of 1.7 eV (corresponding to the wavelength of 600 nm) [41]. These electronic and optical properties make PBnDT-DTBT a good candidate for photovoltaic applications (preliminary BHJ PBnDT-DTBT based solar cells reach PCE of the order of 4 % [41]). In addition to the low band gap and the low HOMO energy level, PBnDT-DTBT has a relatively planar and symmetrical structure (both BnDT and DTBT display high degree of symmetry) which would help promote cofacial $\pi - \pi$ stacking, thus benefiting charge transport. Moreover, PBnDT-DTBT polymer has high molecular weight and good solubility which is due to the long side chains (see Fig. 6.1) [41], both properties enhancing its PCE in solar cells. As in the previous chapters, for the computational time reduction, we substitute the R_1 side chain (3-hexylundecyl) with methyl group (CH_3).

6.1.1 Ground State Structure of PBnDT-DTBT Monomer

Table 6.1 lists the HOMO and LUMO energy levels and their difference for the PBnDT-DTBT monomer in the gas phase and in the considered solvents. The HOMO and LUMO energy levels are more negative in solvents than in the gas phase. Methanol lowers the HOMO energy level of the PBnDT-DTBT monomer the most relative to other solvents. The LUMO energy level is most negative in o-dichlorobenzene

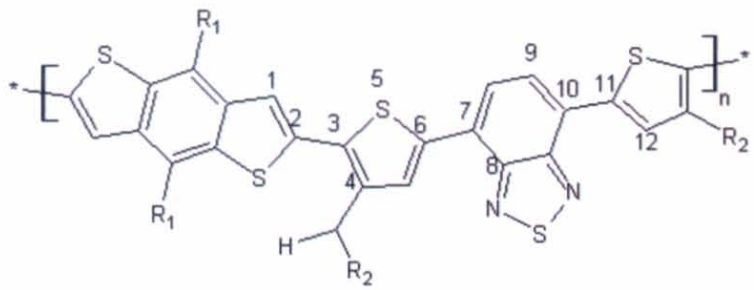

R_1 = 3-hexylundecyl, R_2 = H

Figure 6.1: The chemical structure of the PBnDT-DTBT monomer. 1, 2, 3, ... label the different atoms of the PBnDT-DTBT monomer, that are used in the definitions of the dihedral angles and intra-molecular bonds.

solution. Fig. 6.2 shows the effect of solvents on the HOMO and LUMO energy levels of the PBnDT-DTBT monomer. The HOMO-LUMO energy gap of the PBnDT-DTBT monomer is increased by about 0.1 eV in the solvents in comparison to the gas phase value. The largest $\Delta\varepsilon_{(H-L)}$ is obtained with methanol followed by chloroform, chlorobenzene, and o-dichlorobenzene (see Fig. 6.3). The values in Table 6.1 can be compared to experimental values [41] as discussed above. The HOMO-LUMO energy band gap of 2.4 eV for the monomer compares well with the electrochemical gap of 2.2 eV for PBnDT-DTBT (polymer). Similarly, the HOMO eigenvalue of approximately -5 eV is in a good agreement with the -5.3 eV experimental value. The largest discrepancy is observed for the LUMO eigenvalue (2.7 eV versus 3.2 eV).

Table 6.1: The negative HOMO $-\varepsilon_{HOMO}$ and LUMO $-\varepsilon_{LUMO}$ energy levels and their difference $\Delta\varepsilon_{(H-L)}$ (in eV) for the PBnDT-DTBT monomer using the B3LYP/6-31G^* method.

gas phase /solvent	$-\varepsilon_{HOMO}$	$-\varepsilon_{LUMO}$	$\Delta\varepsilon_{(H-L)}$
gas phase	4.980	2.655	2.325
chloroform	5.069	2.678	2.391
chlorobenzene	5.067	2.688	2.379
o-dichlorobenzene	5.092	2.732	2.36
methanol	5.117	2.687	2.43

Next the ground state geometrical structures of the PBnDT-DTBT monomer are discussed. Table 6.2 lists the dihedral angles Φ, intra-molecular bond lengths r and the electronic dipole moments μ of the PBnDT-DTBT monomers that are calculated using the B3LYP/6-31G^* optimized ground state geometries in the gas phase and in the presence of solvents. As mentioned in Section 6.1 and can be see from Table 6.2, PBnDT-DTBT monomer is nearly planar in its ground state in both the gas

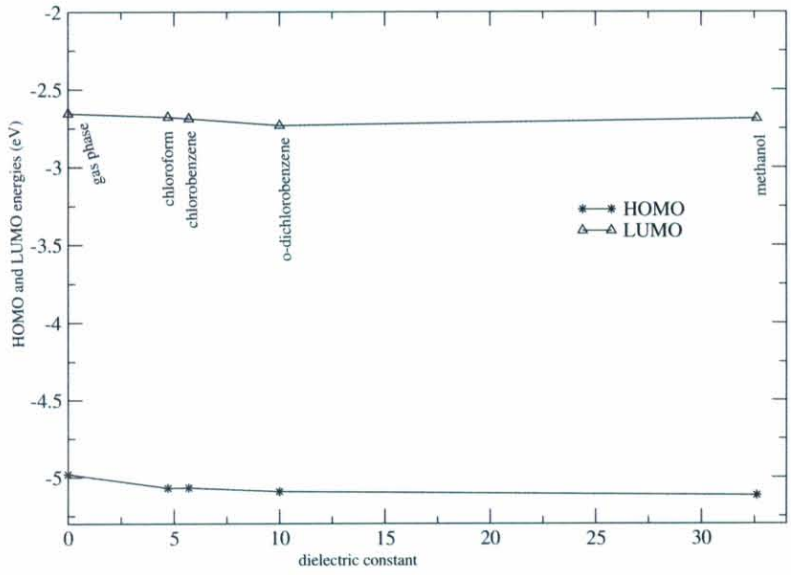

Figure 6.2: The HOMO and LUMO energy levels of the PBnDT-DTBT monomer versus the dielectric constant of solvents.

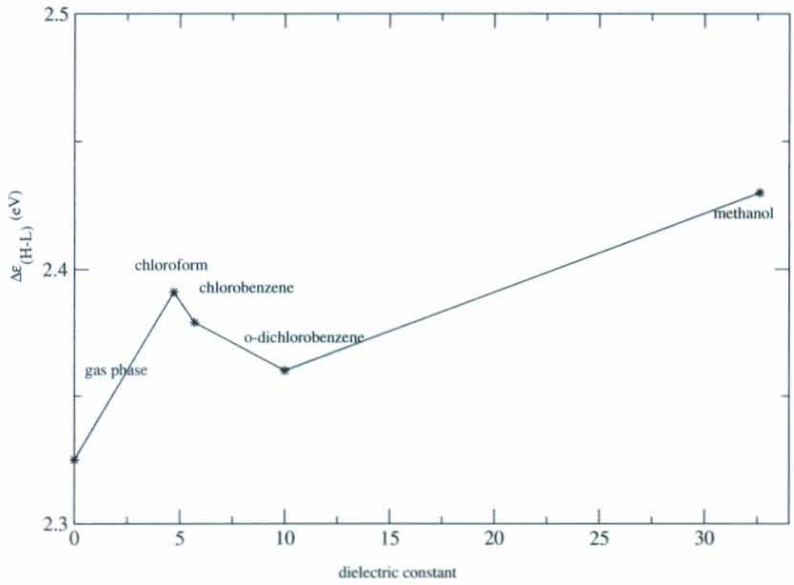

Figure 6.3: The HOMO-LUMO energy gap $\Delta\varepsilon_{H-L}$ of the PBnDT-DTBT monomer versus dielectric constant of solvents.

phase and in the presence of solvents (only $\Phi(1,2,3,4)$ is significantly different from 180°). In most cases, the effect of the solvents is to decrease the planarity of the PBnDT-DTBT monomer somewhat: in chloroform, methanol, and chlorobenzene solutions all three dihedral angles, $\Phi(1,2,3,4)$, $\Phi(5,6,7,8)$, and $\Phi(9,10,11,12)$ are decreased and in o-dichlorobenzene solution $\Phi(5,6,7,8)$ is decreased from $-175°$ to $-172°$, $\Phi(9,10,11,12)$ remains the same and $\Phi(1,2,3,4)$ increases from 159° to 160°. The intra-molecular bond lengths of the PBnDT-DTBT monomer are increased by presence of solvents slightly. As in previous chapters (4 and 5), we can see that the solvents have small effect on the ground state geometries of the polymers studied.

As shown in the Table 6.2 and the Fig. 6.4, the magnitude of the electronic dipole moment μ of the PBnDT-DTBT monomer is increased by the presence of solvents. As is clearly shown in Fig. 6.4, μ does not smoothly (linearly) increase with the polarity of the solvent. In the solvents the magnitude of μ increase, starting from smallest, in the following order: methanol $\rightarrow$ chlorobenzene $\rightarrow$ chloroform $\rightarrow$ o-dichlorobenzene. This order is quite different from what was observed in Chapter 5, where the magnitude of the dipole moment increased with the polarity of the solvent. In contrast, for the PBnDT-DTBT monomer, methanol gives the smallest value (but is still larger than the one obtained for the gas phase) for μ (see Fig. 6.4).

6.1.2 Excited State Properties of PBnDT-DTBT Monomer

The singlet excited state properties of PBnDT-DTBT monomer are also studied using the TD-DFT with the B3LYP/6-31G^* approximation. The lowest excitation energy E_1, the absorption wavelength λ, the oscillator strength f, and the molecular orbital character are listed in the Table 6.3. All transitions from the ground state S_0 to the first excited state S_1 are of HOMO$\rightarrow$LUMO type, with high intensity as suggested

Table 6.2: The dihedral angles Φ (in deg), intra-molecular bond lengths r (in Å) and the electronic dipole moment μ (in Debye) for PBnDT-DTBT monomer as obtained using the B3LYP/6-31G^* method. For the labeling of the angles and bonds see Fig. 6.1.

gas phase /slovent	$\Phi(1,2,3,4)$ r(2,3)	$\Phi(5,6,7,8)$ r(6,7)	$\Phi(9,10,11,12)$ r(10,11)	μ (Debye)
gas phase	158.83 1.448	-175.05 1.454	179.54 1.457	0.4740
chloroform	156.96 1.4494	-170.65 1.455	176.48 1.458	0.5427
chlorobenzene	158.35 1.449	-174.59 1.455	179.39 1.458	0.5057
o-dichlorobenzene	159.66 1.449	-172.51 1.455	179.60 1.458	0.5769
methanol	156.30 1.450	-167.09 1.456	175.29 1.459	0.4944

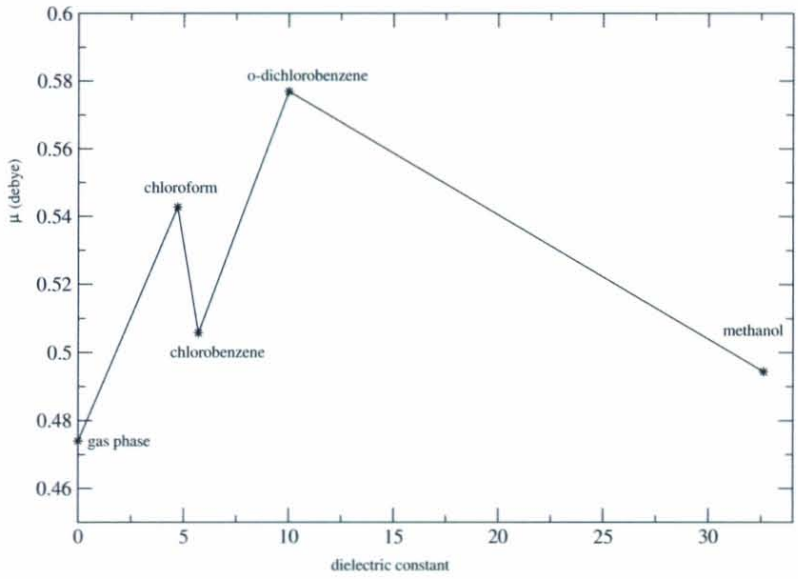

Figure 6.4: The electronic dipole moment of the PBnDT-DTBT monomer versus the solvent dielectric constant.

by f values. E_1 is increased in chloroform and methanol solutions and decreased in chlorobenzene and o-dichlorobenzene solutions. As a result of this behavior of E_1, the λ is blue-shifted in chloroform and methanol, and red-shifted in chlorobenzene and o-dichlorobenzene in reference to the gas phase value (see Figure 6.5). Experimentally, values of 1.7 eV and 600 nm were obtained for E_1 and λ respectively for the PBnDT-DTBT (polymer thin film) in the gas phase and in chloroform solution [41]. In comparison, we have obtained the corresponding values of 2.0 eV for E_1, and 612 and 610 nm for λ in the gas phase and in chloroform respectively. Again as in the case of eigenvalues and their differences, the agreement between theoretical and experimental values is good. The solvent effect on E_1 of PBnDT-DTBT monomer is shown in Fig. 6.5.

6.1.3 Hole Reorganization Energy of PBnDT-DTBT Monomer

PBnDT-based copolymers have recently shown relatively high hole mobility in organic field transistors [99]. However, the PBnDT-DTBT (polymer) still has a relatively low hole mobility of 1.6×10^{-5} cm^2 V^{-1} s^{-1} [41] (for optimal solar cell performance the mobility values should be of the order of 10^{-3} cm^2 V^{-1} s^{-1} or higher). According to Marcus-Hush theory (Chapter 2) studying the hole reorganization energy of polymer will improve our understanding on how to enhance the hole transport in the bulk material such as weakly interacting polymers (such as those considered in this work). Herein, we investigate the solvent effect on the hole reorganization energy of PBnDT-DTBT monomer. Table 6.4 lists λ_h in meV for PBnDT-DTBT monomer. The neutral and radical cation energy levels of PBnDT-DTBT monomer are shown in Fig. 6.6. Among the used solvents, only o-dichlorobenzene decreases λ_h by about 3

Table 6.3: The lowest transition energies E_1, the absorption wavelengths λ, the oscillator strength f, and the molecular orbital character MO of the PBnDT-DTBT monomer using the TD-B3LYP/6-31G^* method.

gas phase /solvent	Transition	E_1 (eV)	λ (nm)	f	MO/Character
gas phase	$S_0 \rightarrow S_1$	2.0264	611.85	0.5361	$HOMO \rightarrow LUMO$
chloroform	$S_0 \rightarrow S_1$	2.0317	610.26	0.7099	$HOMO \rightarrow LUMO$
chlorobenzene	$S_0 \rightarrow S_1$	2.0133	615.83	0.7373	$HOMO \rightarrow LUMO$
o-dichlorobenzene	$S_0 \rightarrow S_1$	1.9961	621.14	0.7264	$HOMO \rightarrow LUMO$
methanol	$S_0 \rightarrow S_1$	2.0485	605.24	0.7049	$HOMO \rightarrow LUMO$

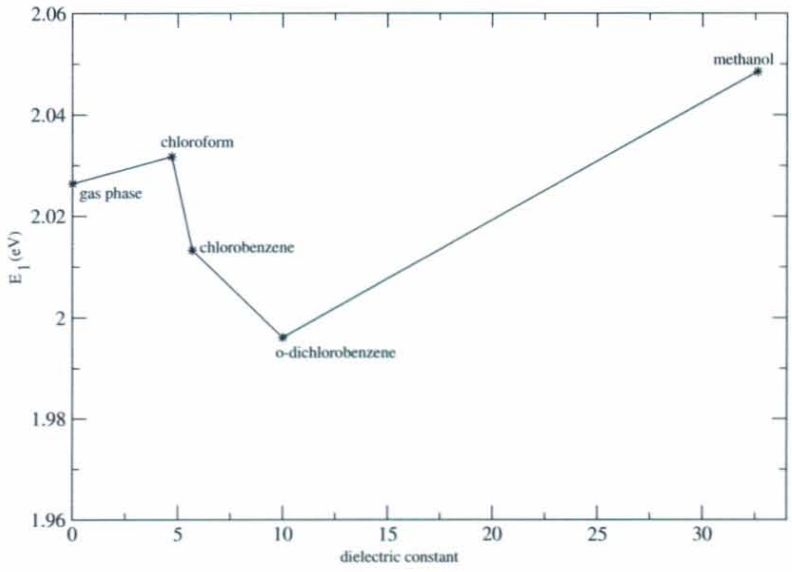

Figure 6.5: The lowest excitation energy E_1 of the PBnDT-DTBT monomer as a function of the dielectric constant of solvents.

meV. Chloroform does not significantly affect λ_h (it increases λ_h by less than 1 meV). Chlorobenzene affects λ_h the most by increasing it by 69 meV with respect to the gas phase value. Methanol, which was the best for enhancing transport rate of PTB7 monomer by lowering λ_h, here works in the opposite direction; it increases the hole reorganization energy by about 10 meV. Hence, of all the solvents considered in this work only o-dichlorobenzene could be a candidate (but just barely) for improving the hole transport of pristine PBnDT-DTBT. Fig. 6.7 shows λ_h of the PBnDT-DTBT monomer versus the solvent dielectric constant.

Table 6.4: The reorganization energy for hole transport of the PBnDT-DTBT monomer in the gas phase and in solvents as calculated using the B3LYP/6-31G^* method.

gas phase /solvent	λ_h (meV)
gas phase	267.16
chloroform	267.94
chlorobenzene	336.36
o-dichlorobenzene	264.28
methanol	277.75

6.2 Conclusions

More negative HOMO and LUMO energy levels and a slightly bigger energy gap of the PBnDT-DTBT monomer are obtained in the presence of the solvents. The electronic ground state dipole moment is increased in the presence of the solvents but it does not increase linearly with the solvent polarity. The lowest singlet-singlet transitions of the PBnDT-DTBT monomer are of $\pi - \pi^*$ type. The lowest excitation energy

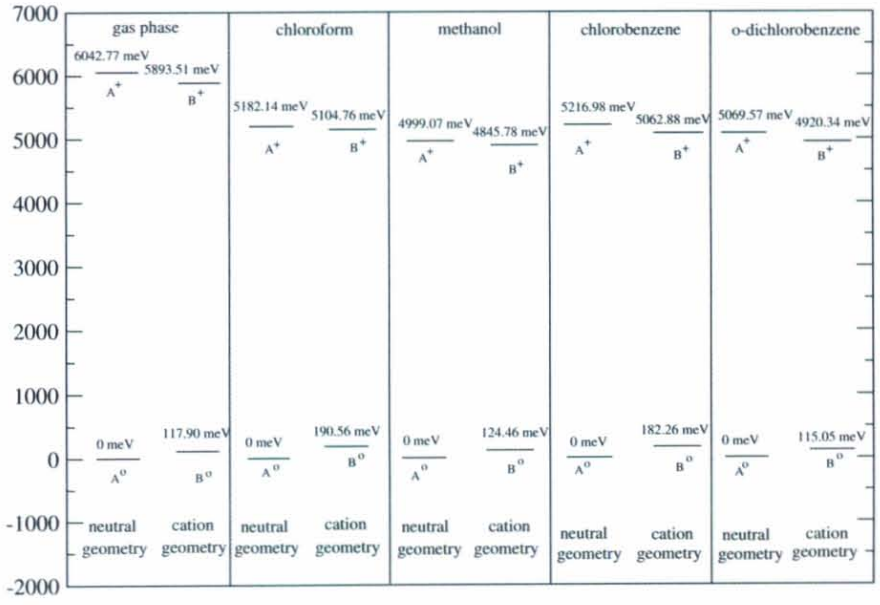

Figure 6.6: The energy levels for the ionic and neutral PBnDT-DTBT monomer in the gas phase and in solvents.

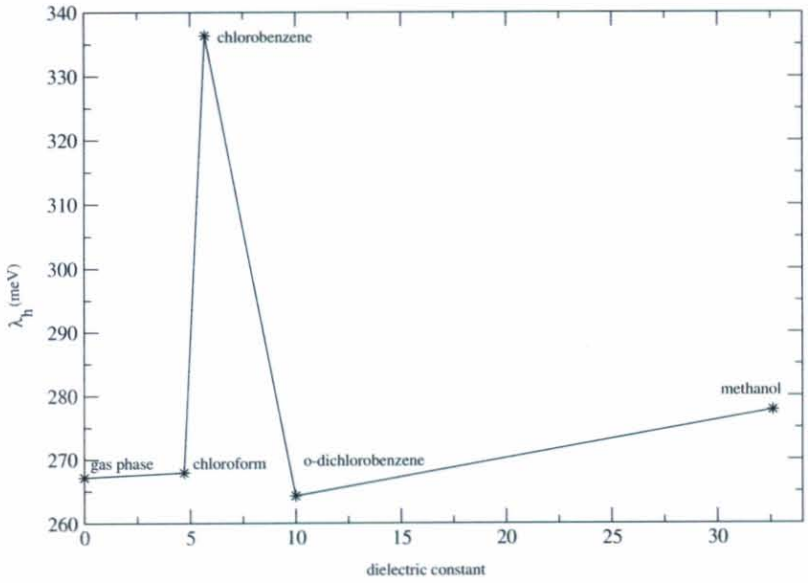

Figure 6.7: The reorganization energy for hole transport λ_h of the PBnDT-DTBT monomer versus the solvent dielectric constant.

is increased in chloroform and methanol solutions so the absorption wavelengths are blue-shifted in these solutions. Chlorobenzene and o-dichlorobenzene decrease E_1 in comparison to the gas phase value, hence, λ is red-shifted in chlorobenzene and o-dichlorobenzene solutions. All considered solvents except o-dichlorobenzene increase the hole reorganization energy of the PBnDT-DTBT monomer with respect to its gas phase value. Hence it would appear that solvents would not have great effect on the either the electronic and optical properties, or the charge transport of the PBnDT-DTBT. However, solvents are still important for the solubility and fabrication of devices.

Chapter 7

Summary and Future Work

The aim of this thesis is to contribute to the understanding of solvent effect on the electronic ground and excited state properties, and charge transport properties of organic conjugated polymers which will hopefully lead to improved the performance of organic devices such as polymer light emitting diodes and solar cells. Some conjugated polymers are soluble in organic solvents and the others are hardly soluble. The solubility of conjugated polymers can be enhanced by attaching longer side chains. Solution-processable organic conjugated polymers are required for low cost thin film fabrication of organic devices.

First, we studied the solvent effect on the ground state HOMO and LUMO energies and their difference of F and C oligomers and the PTB7 and PBnDT-DTBT monomers. The DFT method, which includes the electron correlation beyond the HF approximation, was employed with the hybrid exchange-correlation functional B3LYP and the split-valance polarized basis set 6-31G^*. The PCM model was used to model the solvent effect. Our calculations indicate that for F oligomer, the HOMO and LUMO energy levels are decreased by the solvent; methanol decreases the HOMO and LUMO more than chloroform. The HOMO-LUMO energy gaps are very slightly

lowered by the presence of the solvents for even number of monomers compared to the gas phase. F oligomer has nonplanar structure in the gas phase. Its planarity is enhanced by 1° in chloroform solvent and by 2° in methanol solvent. For the C oligomer, similar to the F oligomer the HOMO and LUMO energy levels are more negative in methanol than in chloroform with respect to the gas phase values. The HOMO-LUMO energy gap of the C oligomer is decreased by the presence of solvent, the effect of chloroform and methanol on the energy gap is more noticeable in the case of C oligomer than of F oligomer. The dihedral angles of the C oligomer are increased in the presence of solvents. Similarly to the F oligomer, the inter-ring distances of the C oligomer are not really affected by chloroform and methanol solvents. For the PTB7 monomer, the same trend as in the F and C oligomers for HOMO and LUMO energy levels is observed, namely they become more negative in the presence of a solvent. The energy gap of the PTB7 monomer is increased in all the considered solvents. The dihedral angles of the PTB7 monomer are virtually unchanged by presence of the solvents. Finally, the ground state energies and structure of the PBnDT-DTBT monomer were also studied in the gas phase and in solvents. More negative HOMO and LUMO energy levels, and wider band gap of the PBnDT-DTBT monomer are obtained in the considered solvents in comparison to the gas phase energies. Some solvents (o-dichlorobenzene) increase the dihedral angles of the PBnDT-DTBT monomer, while the others decrease these angles. The intra-molecular bond lengths of both the PBT7 and the PBnDT-DTBT monomers are not markedly affected by presence of the solvents. While the energies and especially the geometries of the ground states are not affected significantly by the presence of solvents, clearly the magnitudes of the ground state dipole moments are affected even by the nonpolar solvents. In all studied systems, the magnitude of a ground state electronic dipole moment is enhanced by the solvent and in most cases it increases with greater polar-

ity of the solvent (however the actual increase depends on the chemical structure and symmetry of the molecular system).

Second, we concentrate on calculating the lowest singlet-singlet transition energies of the systems in the gas phase and in solvents. The $S_0 \rightarrow S_1$ transitions of all studied systems are HOMO→LUMO transitions, except for the carbazole dimer in which the transitions are of the HOMO-1→LUMO type. The optical band gaps E_1 of F and C oligomers are narrower in the chloroform and methanol solutions than in the gas phase. Except in methanol, E_1 of the PTB7 monomer is increased. Chlorobenzene and o-dichlorobenzene solvents decrease E_1 of the PBnDT-DTBT monomer, but chloroform and methanol increase it.

Third, we focused on the effect of the solvent on the hole reorganization energy λ_h of the PTB7 and the PBnDT-DTBT monomers. λ_h of the PTB7 monomer is decreased by the presence of the solvent and decreased most in methanol compared to the gas phase. In contrast, λ_h of the PBnDT-DTBT monomer is mostly increased by the solvents. Only in o-dichlorobenzene, λ_h is decreased. Among the considered solvents, methanol is the best for hole transport of PTB7 monomer, and o-dichlorobenzene is the best for hole transport of PBnDT-DTBT monomer.

To summarize, the proposed computational approaches show that more negative HOMO and LUMO energy levels of conjugated polymers are obtained with the solvent. The HOMO-LUMO energy gap is slightly affected by the solvent. Generally, the polarity of the solvent increases the dipole moment of conjugated polymers. In most cases, a wider range of absorption wavelengths are obtained in the presence of solvents. Some solvents have a promising effect on the transport properties of conjugate polymers. For example, the work in thesis shows that including the external contributions in the calculations of the reorganization energy needs to be more carefully investigated in order to improve our understanding of a solvent effect on the

reorganization energy (and hence charge transport) of conjugated polymers.

It should be pointed out that, for the conjugated polymers, there remain many research areas to be investigated in order to fully understand the effect of a solvent on their properties and applications in different devices. Studying the solvent effect on the morphology of conjugated polymer can give a better idea on how the solvent effect the transport properties. Fuller investigation of a solvent effect on the charge carrier mobility of conjugated polymers is essential for further improvements in getting cheaper and easier fabrication of solution-processable devices. It would also be useful to use different solvation models to study the solvent effect in order to see which model gives more accurate results.

Bibliography

[1] T. J. Skotheim, *Handbook of Conducting Polymers*, Vols. 1 and 2, M. Dekker Inc. New York (1986).

[2] K. Ogawa, and S. C. Rasmussen, *N-Functionalized Poly(Dithieno[3,2-b:2',3'-d]Pyrrol)s: Highly Fluorescent Materials with Reduced Band Gap*, Macromolecules, 39, 1771 (2006).

[3] C. K. Chiang, C. R. Fincher, Jr., Y. W. Park, and A. J. Heeger, *Electrical Conductivity in Doped Polyacetylene*, Phys. Rev. Lett. 39, 1098 (1977).

[4] H. Shirakawa, A. MacDiarmid, and A. Heeger, *Twenty-Five Years of Conducting Polymers*, Chem. Commun. 1, (2003).

[5] J. H. Burroughes, D. D. C. Bradley, A. R. Brown, R. N. Marks, K. Mackay, R. H. Friend, P. L. Burns. and A. B. Holmes, *Light-Emitting Diodes Based on Conjugated Polymers*, Nature. 347, 539 (1990).

[6] A. Kraft, C. Grimsdale, and A. B. Holmes, *Electroluminescent Conjugated Polymers-Seeing Polymers in a New Light*, Angew. Chem. Int. Ed. 37, 402 (1998).

[7] N. C. Greenham, S. C. Moratti, D. D. C. Bradley, R. H. Friend, and A. B. Holmes, *Efficient Light-Emitting Diodes Based on Polymers with High Electron Affinities*, Nature. 365, 628 (1993).

[8] Y. Ohmori, M. Uchida, K. Muro, and K. Yoshino, *Effect of Alkyl Chain Length and Carrier Confinement Layer on Characteristics od Poly(3-alkylthiophene) electroluminescent Diodes*, Solid State Communications, 80, 605 (1991).

[9] S. Doi, M. Kuwabara, T. Noguchi, and T. Ohnishi, *Organic Electroluminescent Devices having Poly(dialkoxy-p-phenylene vinylenes) as A Light Emitting Material*, Synthetic Metals, 57, 4174 (1993).

[10] N. Tada, A. Fujii, Y. Ohmori, Member, IEEE, and K. Yoshino, *Multicolor Organic Electroluminescent Device Utilizing Vapor-Deposited Fluorescent Dye Films*, IEEE Transactions on Electron Devices, 44, 1234 (1997).

[11] Y. Ohmori, N. Tada, A. Fujii, H. Ueta, T. Sawatani, and K. Yoshino, *Organic Electroluminescent Device with R-G-B Emission*, Thin Solid Films, 331, 89 (1998).

[12] L. Akcelrud, *Electroluminescent Polymers*, Progress in Polymer Science, 28, 875 (2003).

[13] S. Sinha, and A. P. Monkman, *Effect of Electric Field, Solvent, and Concentration on the Electroluminescence Spectra and Performance of Poly[2-methoxy-5-(2'-ethyl-hexyloxy)-1,4-phenylene vinylene] Based Light Emitting Diodes*, J. Appl. Phys. 93, 5691 (2003).

[14] Y. Shu, J. Liu, and Y. Yang, *Device Performance and Polymer Morphology in Polymer Light Emitting Diodes: The Control of Thin Film Morphology and Device Quantum Efficiency.* J. Appl. Phys. 87, 4254 (2000).

[15] J. Liu, Y. Shi, L. Ma, and Y. Yang, *Device Performance and Polymer Morphology in Polymer light emitting Diodes: The Control of Device Electrical Properties and Metal/Polymer Contact*, J. Appl. Phys. 88, 605 (2000).

[16] L.-W. Chong, T.-C. Wen, Y.-L. Lee, and T.-F. Guo, *The Modification of Silver Anode by an Organic Solvent (Tetrahydrofuran) for Top-Emissive Polymer Light-Emitting Diodes*, Organic Electronics, 9, 515 (2008).

[17] T. G.-Abe. F. Pschenitzka, H. Z. Jin, B. Bollman, and J. C. Sturm, *Solvent-Enhanced Dye Diffusion in Polymer Thin Films for Polymer Light-Emitting Diode Application*, J. Appl. Phys. 96, 7154 (2004).

[18] S. Xiao, C. Qiu, E. Jin, Y. Chen, P. Louis, S. Qiu, W.-W. Zhu, M. Nguyen, and I. Shih, *Effects of Solvent on Fabrication of Polymeric Light Emitting Devices*, Material Lett. 59, 694 (2005).

[19] P. Poolmee, M. Ehara, S. Hannongbua, and H. Nakatsuji, *SAC-CI Theoretical Investigation on Electronic Structure of Fluorene-Thiophene Oligomers*, Polymer, 46, 6474 (2005).

[20] D.-H. Hwang, M.-J. Park, J.-H. Lee, *EL Properties of Stable Blue Light-Emitting Polyfluorene Copolymers*, Materials Science and Engineering C. 24, 201 (2004).

[21] W. Wu, M. Inbasekaran, M. Hudack, D. Welsh, W. Yu, Y. Cheng, C. Wang, S. Kram, M. Tacey, M. Bernius, R. Fletcher, K. Kiszka, S. Munger, and J.

O'Brien, *Recent Development of Polyfluorene-Based RGB Materials for Light Emitting Diodes*, Microelectronic Journal, 35, 343 (2004).

[22] S. M. Bonesi, and R. Erra-Balsells, *Electronic Spectroscopic of Carbazole and N- and C-Substituted Carbazoles in Homogeneous Media and in Solid Matrix*, Jounral of Luminescence, 93, 51 (2001).

[23] E. E. Romero-Ale, A. L. Olives, M. A. Martín, B. D. Castillo, P. López-Alvarado, and J. C. Menéndez, *Environmental Effects on the Fluorescence Behaviour of Carbazole Derivatization Reagents*, Luminescence, 20, 162 (2005).

[24] T. S. Spencer, and C. M. O'Donnell, *Energy Transfer in a Hydrogen-Bonded Carbazole-Benzophenone Complex*, J. Am. Chem. Soc. 94:14, 4846 (1972).

[25] M. S. Bratcher, M. S. DeClue, A. Grunnet-Jepsen. D. Wright, B. R. Smith, W. E. Moerner, and J. S. Siegel, *Synthesis of Bifunctional Photorefractive Polymers with Net Gain: Desin Strategy Amenable to Combinatorial Optimization*, J. Am. Chem. Soc. 120, 9680 (1998).

[26] R. Janssen *Introduction to Polymer Solar Cells*, Ph. D. thesis, Eindhoven Unversity of Technology, The Netherlands.

[27] K. M. Coakley, and M. D. McGehee, *Conjugated Polymer Photovoltaic Cells*, Chem. Mater. 16, 4533 (2004).

[28] W. Ma, C. Yang, X. Gong, K. Lee, and A. J. Heeger, *Thermally Stable, Efficient Polymer Solar Cells with Nanoscale Control of the Interpenetrating Network Morphology*, Adv. Funct. Mater. 15, 1617 (2005).

[29] G. Li, Y. Yao, H. Yang, V. Shrotriya, G. Yang, and Y. Yang, *Solvent Annealing Effect in Polymer Solar Cells Based on Poly(3-hexylthiophene) and Methanol-fullerenes*, Avd. Funct. Mater. 17, 1636 (2007).

[30] M. Reyes-Reyes, K. Kim, and D. L. Carroll, *High-Efficiency Photovoltaic Devices Based on Annealed Poly(3-hexylthiophene) and 1-(3-methoxycarbonyl)-prpyl-1-phenyl-(6,6)C61 Blends*, Appl. Phys. Lett. 87, 083506 (2005).

[31] C.-H. Hsieh, Y.-J. Cheng, P.-J. Li, C.-H. Chen, M. Dubosc, R.-M. Liang, and C.-S. Hsu, *Highly Efficient and Stable Inverted Polymer Solar Cells Integrated with a Cross-Linked Fullerene Material as an Interlayer*, J. Am. Chem. Soc. 132, 4887 (2010).

[32] A. P. Zoombelt, M. A. M. Leenen, M. Fonrodona, Y. Nicolas, M. M. Wienk, and R. A. J. Janssen, *The Influence of Side Chains on Solubility and Photovoltaic Performance of Dithiophene-Thienopyrazine Small Band Gap Copolymers*, Polymer. 50, 4564 (2009).

[33] B. C. Thompson, and M. J. Fréchet, *Polymer-Fullerene Composite Solar Cells*, Angew. Chem. Int. Ed. 47, 58 (2008).

[34] G. Yu, J. Gao, J. C. Hummelen, F. Wudl, and J. Heeger, *Polymer Photovoltiac Cells: Enhanced Efficiencies via a Network of Internal Donor-Acceptor Heterojunctions*, Science, 270, 1789 (1995).

[35] C. J. Brabec, N. S. Sariciftci, and J. C. Hummelen, Plastic Solar Cells, Adv. Funct. Meter. 11, 15 (2001).

[36] C. Dennler, M. C. Scharber, and C. J. Brabec, *Polymer-Fullerene Bulk-Heterojunction Solar Cells*, Adv. Mater. 21, 1323 (2009).

[37] J. Peet, A. J. Heeger, and G. C. Bazan, *Plastic Solar Cells: Self-Assembly of Bulk Heterojunction Nanomaterials by Spontaneous Phase Separation*, Accounts of Chemical Research, 42, 1700 (2009).

[38] C. H. Woo, B. C. Thompson, B. J. Kim, M. F. Toney, and J. M. J. Fréchet, *The Influence of Poly(3-hexylthiophene) Regioregularity on Fullerene-Composite Solar Cell Performance*, J. Am. Chem. Soc. 130, 16324 (2008).

[39] G. Li, V. Shrotriya, J. Huang, Y. Yao, T. Moriarty, K. Emery, and Y. Yang, *—High-Efficiency Solution Processable Polymer Photovoltiac Cells by Self-Organization of Polymer Blends*, Nature Materials, 4, 864 (2005).

[40] Y. Laing, Z. Xu, J. Xia, S. Tsai, Y. Wu, G. Li, C. Ray, and L. Yu, *For the Bright Future-Bulk Heterojunction Polymer Solar Cells with Power Conversion Efficiency of 7.4%*, Adv. Mater. 22, E135 (2010).

[41] S. C. Price, A. C. Stuart, and W. You, *Low Band Gap Polymers Based on Benzo[1,2-b:4,5-b']dithiophene: Rational Design of Polymer Leads to High Photovoltiac Performance*, Macromolecules, 43, 4609 (2010).

[42] (a) Relative Permittivity-Wikipedia, the free encyclopedia, (b) Solvent-Wikipedia, the free encyclopedia.

[43] J. Kohanoff, *Electronic Structure Calculations for Solids and Molecules*, Cambridge University Press, UK, (2006).

[44] W. Koch, M. C. Holthausen, *A Chemist's Guide to Density Functional Theory*, Second Edition, Wiley-Vch, (2001).

[45] W. Kohn, L. J. Sham, *Self-Consisten Equations Including Exchange and Correlation Effect*, Phys. Rev. 140, 4A, 1133 (1965).

[46] W. Kohn, A. D. Becke, and R. G. Parr, *Density Functional Theory of Electronic Structure*, J. Phys. Chem. 100, 12974 (1996).

[47] M. Betzinger, C. Friedrich, and S. Blügel, *Hybrid Functionals within the All-Electron FLAPW Method: Implementation and Applications of PBE0*, Phys. Rev. B. 81, 195117 (2010).

[48] A. D. Becke, *Density -Functional Thermochemsitry. III. The Role of Excat Exchange*, J. Chem. Phys. 98(7), 5648 (1993).

[49] P. J. Stephens, F. J. Devlin, C. F. Chabalowski, and M. J. Frisch, *Ab Initio Calculation of Vibrational Absorption and Circular Dichroism Spectra Using Density Functional Force Fields*, J. Phys. Chem. 98, 11623 (1994).

[50] J. P. Perdwe, *In Electronic Structure of Solid*, Akademie Verlag, Berlin, (1991).

[51] S. H. Vosko, L. Wilk, and M. Nusair, *Accurate Spin-Dependent Electron Liquid Correlation Energies for Local Spin Density Calculations: A Critical Analysis*, Can. J. Phys. 58, 1200 (1980).

[52] C. Lee, W. Yang, and R. G. Parr, *Development of Colle-Salvetti Correlation-Energy Formula into A Functional of The Electron Density*, Phys. Rev. B. 37, 785 (1988).

[53] M. J. Frisch, G. W. Trucks, H. B. Schlegel, G. E. Scuseria, M. A. Robb, J. R. Cheeseman, J. A. Montgomery, Jr., T. Vreven, K. N. Kudin, J. C. Burant, J. M. Millam, S. S. Iyengar, J. Tomasi, V. Barone, B. Mennucci, M. Cossi, G. Scalmani, N. Rega, G. A. Petersson, H. Nakatsuji, M. Hada, M. Ehara, K. Toyota, R. Fukuda, J. Hasegawa, M. Ishida, T. Nakajima, Y. Honda, O. Kitao, H. Nakai, M. Klene, X. Li, J. E. Knox, H. P. Hratchian, J. B. Cross, V.

Bakken, C. Adamo, J. Jaramillo, R. Gomperts, R. E. Stratmann, O. Yazyev, A. J. Austin, R. Cammi, C. Pomelli, J. W. Ochterski, P. Y. Ayala, K. Morokuma, G. A. Voth, P. Salvador, J. J. Dannenberg, V. G. Zakrzewski, S. Dapprich, A. D. Daniels, M. C. Strain, O. Farkas, D. K. Malick, A. D. Rabuck, K. Raghavachari, J. B. Foresman, J. V. Ortiz, Q. Cui, A. G. Baboul, S. Clifford, J. Cioslowski, B. B. Stefanov, G. Liu, A. Liashenko, P. Piskorz, I. Komaromi, R. L. Martin, D. J. Fox, T. Keith, M. A. Al-Laham, C. Y. Peng, A. Nanayakkara, M. Challacombe, P. M. W. Gill, B. Johnson, W. Chen, M. W. Wong, C. Gonzalez, and J. A. Pople, *Gaussian 03*, Gaussian, Inc., Pittsburgh PA, (2003).

[54] J. Baker, and P. Pulay, *Assessment of The Handy-Cohen Optimized exchange Density Functional for Organic Reactions*, J. Chem. Phys. 117, 1441 (2002).

[55] C. C. J. Roothaan, *New Developments in Molecular Orbital Theory*, Rev. Mod. Phys. 23, 69 (1951).

[56] J. B. Foresman, and A. Frisch, *Exploring Chemistry with Electronic Structure Methods*, second edition, Gaussian, Inc. Pittsburgh, PA (1996).

[57] E. Runge, and E. K. U. Gross, *Density-Functional Theory for Time-Dependent Systems*, Phys. Rev. Lett. 52, 997 (1984).

[58] M. A. L. Marques, and E. K. U. Gross, *Time-Dependent Density Functional Theory*, Annu. Rev. Phys. Chem. 55,427 (2004).

[59] L. J. Bartolotti, *Time-Dependent Extension of The Hohenberg-Kohn-Levy*, Phys. Rev. A. 24, 1661 (1981).

[60] V. Peuckert, *A New Approximation Method for Electron Systems*, J. Phys. c: solid state Phys. 11, 4945 (1978).

[61] L. V. Keldysh, *Diagram Technique for Nonequilibrium Processes*, Sov. Phys. JETP. 20, 1018 (1965).

[62] B. Mennucci, *Solvation Effect on Molecules and Biomolecules*, Pisa, Italy (2008).

[63] V. Barone, and M. Cossi, *A New Definition of Cavities for the Computation of Solvation Free Energies by The Polarizable Continuum Model*, J. Chem. Phys. 107(8), 3210 (1997).

[64] E. Cancés, B. Mennucci, and J. Tomasi, *A New Integral Equation Formalism for The Polarizable Continuum Model: Theoretical Background and Applications to Isotropic and Anisotropic Dielectric*, J. Chem. Phys. 107(8), 3032 (1997).

[65] M. Cossi, N. Rega, G. Scalmani, and V. Barone, *Polarizable Dielectric Model of Solvation wuth Inclusion of Charge Pentration Effects*, J. Chem. Phys. 114, 5691 (2001).

[66] M. Cossi, G. Scalmani, N. Rega, and V. Barone, *New Developments in The Polarizable Continuum Model for Quantum Mechanical and Classical Calculations on Molecules in Solution*, J. Chem. Phys. 117, 43 (2002).

[67] W. Hackbusch, *Integral Equations-Theory and Numerical Treatment*, Birkhäuser Vrlag, Basel, Switzerland, (1995).

[68] B. Mennucci, and R. Cammi, *Continuum Solvation Models in Chemical Physics From Theory to Applications*, John Wiley & Sons, Ltd, England (2007).

[69] R. A. Marcus, *Electron Transfer Reactions in Chemsitry. Theory and Expermint*, Rev. Mod. Phys. 65, 599 (1993).

[70] M. Malagoli, and J. L. Bredas, *Density Functional Theory Study of The Geometric Structure and Energies of Triphenylamine-Based Hole-Transporting Molecules*, Chem. Phys. Lett. 327, 13 (2000).

[71] *Gaussian 09 User Reference* www.gaussian.com.

[72] W. J. Hehre, L. Radom, P. V. R. Schleyer, and J. A. Pople, *AB Initio Molecular Orbital Theory*, Wiley Interscience, New York (1985).

[73] Z. Gong, and J. B. Lagowski, *Density Functional Study of the Electronic and Optical Properties of Fluorene-Thieno[3,2-b]Thiophene-Based Conjugated Copolymers*, Molecular Simulation, 35, 737 (2009).

[74] A. E. Frisch, R. D. Dennington II, T. A. Keith, A. B. Nielsen, and A. J. Holder, *Gauss View Reference*, Gaussian Inc. Pittsburgh, PA (2003).

[75] J. Pei, W. Yu, W. Huang, and A. J. Heeger, *The Synthesis and Characterization of an Efficient Green Electroluminescent Conjugated Polymer: Poly[2,7-Bis(4-Hexylthienyl)-9,9-Dihexylfluorene]*, Chem. Commun. 1631 (2000).

[76] M. Belletête, S. Beauprè, J. Bouchard, P. Blondin, M. Leclerc, and G. Durocher, *Theoretical and Experimnetal Investigations of the Spectroscopic and Photophysical Properties of Fluorene-Phenylene and Fluorene-Thiophene Derivatives: Precursors of Light-Emitting Polymers*, J. Phys. Chem. B. 104, 9118 (2000).

[77] J. Hwang, E. Kim, J. Liu, J. Brédas, A. Duggal, and A. Kahn, *Photoelectron Spectroscopic Study of the Electronic Band Structure of Polyfluorene and Fluorene-Arylamine Copolymer at Interfaces*, J. Phys. Chem. C. 111, 1378 (2007).

[78] P. Chen, G. Yang, T. Liu, T. Li, M. Wang, and W. Huang, *Optimization of Opto-Electronic Properties and Dvice Efficiency of Polyfluorenes by Tuning Structure and Morphology*, Polymer Int. 55, 473 (2006).

[79] J. Wang, J. Feng, A. Ren, X. Liu, Y. Ma, P. Lu, and H. Zhang, *Theoretical Studies of the Absorption and Emission Properties of the Fluorene-Based Conjugated Polymers*, Macromolecules, 37, 3451 (2004).

[80] M. Belletête, S. Beauprè, J. Bouchard, P. Blondin, M. Leclerc, and G. Durocher, *Theoretical and Expermintal Investigations of The Spectroscopic and Photophysical Properties of Fluorene-Phenylene and Fluorene-Thiophene Derivatives: Precursors of Light-Emitting Polymers*, J. Phys. Chem. B. 104, 9118 (2000).

[81] W. P. Anderson, W. D. Edwards, and M. C. Zerner, *Calculated Spectra of Hydrated Ions of the First Transition-Metal Series*, Inorg. Chem. 25, 2728 (1986).

[82] M. A. Thompson, and M. C. Zerner, *A Theoretical Examination of the Electronic Structure and Spectroscopy of the Photosynthetic Reaction Center from Rhodopseudomonas Viridis*, J. Am. Chem. Soc. 113, 8210 (1991).

[83] H. Hoegl, *On Photoelectric Effect in Polymers and Their Sensitization by Dopants*, J. Phys. Chem. 69, 755 (1965).

[84] S. M. Zain, R. Hashim, A. G. Taylor, and D. Phillips, *Electronic Structures of Carbazole and its Derivatives: A semi-Empirical Study on the Substitution Effect of Carbazole*, J. Mol. Struct. (Theochem). 401, 287 (1997).

[85] N. Blouin, A. Michaud, and M. Leclerc, *A Low-Bandgap Poly(2,7-Carbazole) Derivative for Use in High-Performance Solar Cells*, Adv. Mater. 19, 2295 (2007).

[86] Y. Zou, D. Gendron, R. Badrou-Aïch, A. Najari, Y. Tao, and M. Leclerc, *A High-Mobility Low-Bandgap Poly(2,7-Carbazole) Derivative for Photovoltiac A pplications*, Macromolecules, 42, 2891 (2009).

[87] L. Yang, J. Feng, A. Ren, and J. Sun, *The Electronic Structure and Optical Properties of Carbazole-Based Conjugated Oligomers and Polymers: A Theoretical Investigation*, Polymer, 47, 1397 (2006).

[88] G. Zotti, G. Schiavon, S. Zecchin, J.-F. Morin, and M. Leclerc, *Electrochemical, Conductive, and Magnetic Properties of 2,7-Carbazole-Based Conjugated Polymers*, Macromolecules, 35, 2122 (2002).

[89] H. Zhou, L. Yang, S. C. Price, K. J. Knight, and W. You, *Enhanced Photovoltiac Performance of Low-Bandgap Polymers with Deep LUMO Levels*, Angew. Chem. Int. Ed. 49, 7992 (2010).

[90] M. C. Scharber, D. Mühlbacher, M. Koppe, P. Denk, C. Waldauf, A. J. Heeger, and C. J. Brabec, *Design Rules for Donors in Bulk-Heterojunction Solar Cells-Toward 10% Energy-Conversion Efficiency*, Adv. Mater. 18, 789 (2006).

[91] Z. Gong, and J. B. Lagowski, *Theoretical Study of The Structure and Electronic Properties of the Dimer of Fluorene and Carbazole and Their Derivatives*, J. Mol. Struct. (Theochem). 866, 27 (2008).

[92] M. Belletête, M. Bédard, M. Leclerc, and G. Durocher, *Ground and Excited State Properties of Carbazole-Based Dyads: Corre;ation with Their Respective Absorption and Fluorescence Spectra*, J. Mol. Struct. (Theochem). 679, 9 (2004).

[93] Y. Chen. T. Yamamura, and K. Igarashi, *Photosensitization of Carbazole Derivatives in Cationic Polymerization with a Novel Sensitivity to Near-UV Light*, Journal of Polymer Science: Part A: Polymer Chemistry, 38, 90 (2000).

[94] Y. Liang, D. Feng, Y. Wu, S. Tsai, G. Li, and C. Ray, *Highly Efficient Solar Cell Polymers Developed via Fine-Tuning of Structural and Electric Properties*, J. Am. Chem. Soc. 131, 7792 (2009).

[95] R. S. Sánchez-Carrera, *Theoretical Characterization of Charge Transport in Organic Molecular Crystals*, PHD online thesis, Georgia Institute Technology (2008).

[96] J. Kürti, P. R. Surjàn, and M. Kertesz, *Electronic Structure and Optical Absorption of Poly(biisothianaphthene-methine) and Poly(isonaphthothiophene-thiophene): Two Low-Band Gap Polymers*, J. Am . Chem. Soc. 113, 9865 (1991).

[97] M. Jayakannan, P. A. Van Hal, R. A. J. Janssen, *Synthesis, Optical, and Electrochemical Properties of Novel Copolymers on the Basis of Benzothiadiazole and Electron-Rich Arene Units*, Journal of Polymer Science: Part A: Polymer Chemistry, 40, 2360 (2002).

[98] E. V. Keuren, H. Möhwald, S. Rozouvan, W. Schrof, V. Belov, H. Matsuda, and S. Yamada, *Linear and Third Order Nonlinear Optical Properties of Substituted Oligothiophenes*, J. Chem. Phys. 110, 3584 (1999).

[99] H. Pan, Y. Li, Y. Wu, P. Liu, B. S. Ong, S. Zhu, and G. Xu, *Low-Temperature, Solution-Processed, High-Mobility Polymer Semiconductors for Thin-Film Transistors*, J. Am. Chem. Soc. 129, 4112 (2007).